JGR Solid Earth

RESEARCH ARTICLE
10.1029/2022JB025983

The Moho Architecture and Its Role for Isostasy—Insights From the Lofoten-Vesterålen Rifted Margin, Norway

Christian Schiffer[1], **Stéphane Rondenay**[2], **Lars Ottemöller**[2], **and Anne Drottning**[2]

[1]Department of Earth Sciences, Uppsala University, Uppsala, Sweden, [2]Department of Earth Science, University of Bergen, Bergen, Norway

Key Points:

- Receiver function inversion in Nordland and Troms, Northern Norway confirms earlier crustal structure models
- Topography in the Lofoten-Vesterålen archipelago is not isostatically compensated from within the crust and requires additional buoyancy
- A newly discovered low-density layer in the uppermost mantle beneath the Lofoten-Vesterålen archipelago provides the additional buoyancy

Supporting Information:

Supporting Information may be found in the online version of this article.

Correspondence to:

C. Schiffer,
christian.schiffer@geo.uu.se

Citation:

Schiffer, C., Rondenay, S., Ottemöller, L., & Drottning, A. (2023). The Moho architecture and its role for isostasy—Insights from the Lofoten-Vesterålen rifted margin, Norway. *Journal of Geophysical Research: Solid Earth*, *128*, e2022JB025983. https://doi.org/10.1029/2022JB025983

Received 7 NOV 2022
Accepted 22 APR 2023

Author Contributions:

Conceptualization: Christian Schiffer, Stéphane Rondenay, Anne Drottning
Data curation: Christian Schiffer, Stéphane Rondenay, Lars Ottemöller
Formal analysis: Christian Schiffer, Anne Drottning
Investigation: Christian Schiffer, Anne Drottning
Methodology: Christian Schiffer, Stéphane Rondenay, Anne Drottning
Supervision: Christian Schiffer, Stéphane Rondenay, Lars Ottemöller
Validation: Christian Schiffer, Stéphane Rondenay, Lars Ottemöller

Abstract The crustal structure of the Nordland and Troms region, Norway, has received growing scientific attention because (a) the region is one of the most seismically active areas of mainland Norway, and (b) there are differing interpretations of the crustal structure but none of the proposed models simultaneously satisfy gravity, topography and crustal isostasy. At the core of the puzzle is the Lofoten-Vesterålen archipelago, which exhibits considerable variations in crustal thickness, seemingly inconsistent with the topographic expression along this geomorphic structure. The prevalent view has been that the crust beneath the southern Lofoten is extremely thin (~20 km). This has recently been disputed. Here, we address this debate by producing new lithospheric models in the region from joint inversion of receiver functions and P-wave polarizations at 62 seismic stations. Our results are consistent with the regional trends from other models, including a shallow Moho in the southern Lofoten. Moreover, our results detect a low-velocity layer in the uppermost mantle, which appears to be highly relevant to isostasy in the region. We conclude that the crustal structure in the region may not be as controversial as the recent debate suggested. What appears more urgent to understand is how the concept of isostasy is defined, and how it relates to the layered structure of the lithosphere. In particular, our findings emphasize the importance of conceptualizing the Moho as a transition zone with considerable thickness and internal structural variations, rather than a simple velocity discontinuity.

Plain Language Summary The Nordland and Troms region, Norway, is one of the most seismically active areas of mainland Norway. To understand the occurrence of earthquakes, we need to understand the forces acting on and in the tectonic plate, the lithosphere, which consists of the crust and the underlying lithospheric mantle. One set of forces are caused by the distribution of masses and thereby variations of potential energy within the lithosphere. However, in the study area the structure of the lithosphere and the internal mass distribution is debated. So far, none of the proposed models can satisfactorily explain the geological observations. In particular the crust and topography seem to have a paradoxical relation. To gather more information, we develop another complementary model of the lithospheric structure based on a seismological method not yet applied in the area to this extent. Our new seismological study roughly confirms previous models of the crust. However, the model includes a hitherto unseen structure beneath the crust that may be key to understanding the relationship between topography and crust. This may have general and global implications for lithospheric structure.

1. Introduction

Rifted continental margins are complex zones of transition between continental to oceanic lithosphere. They are often formed by multiple episodes of continental rifting, which ultimately result in the breakup of continental lithosphere (Bradley, 2008; Franke, 2013). The structure of rifted continental margins can be very complex and include (a) variations in crustal thickness, including ribbons, horst and graben structures, and hyperextension (e.g., Gernigon et al., 2020; Péron-Pinvidic & Manatschal, 2010); (b) exhumation of mantle lithosphere (Péron-Pinvidic & Manatschal, 2010; Sibuet, 1992); (c) various amounts of volcanic products (e.g., Franke, 2013; Thybo & Artemieva, 2013); and (d) *so-called* lower crustal bodies, or high velocity/density lower crust (e.g., Gernigon et al., 2004; from now on called *high velocity lower crust*, or HVLC). HVLC is predominantly observed in wide-angle refraction studies across rifted continental margins, with characteristic P-wave velocities (Vp) of typically ~7.1–7.6 km/s, and is usually associated with higher-than-normal (crustal) densities. Such HVLC is not confined to continental margins. For example, it can be found in former collision/suture zones, as well as in cratonic crust or in rift zones (e.g., Schulte-Pelkum et al., 2017; Thybo & Artemieva, 2013).

Visualization: Christian Schiffer
Writing – original draft: Christian Schiffer, Stéphane Rondenay
Writing – review & editing: Christian Schiffer, Stéphane Rondenay, Lars Ottemöller

The origin of HVLC is debated and likely varies between geodynamic settings. Some of the proposed models include magmatic underplating or intrusions, hydrated peridotite, pre-existing metamorphosed mafic crust or peridotite (e.g., Gernigon et al., 2004). Although peridotite is not a crustal lithology, we will still address this possibility by the expression HVLC. The existence of HVLC, compounded by its uncertain lithology and origin, complicates the process of defining a Moho discontinuity (e.g., Mjelde et al., 2013; Thybo & Artemieva, 2013). Many global or regional studies currently depend on lithospheric models that include a clearly defined Moho. However, because of structural complications surrounding the Moho, it may be more viable to define the Moho as a three-dimensional crust-mantle transition zone with internal structure.

In this study we investigate this problem with a case study of the Nordland and Troms region of Northern Norway (Figure 1). The study region comprises the narrow Lofoten-Vesterålen continental rifted margin hosting Permian-Triassic to Cretaceous sedimentary basins, the Lofoten-Vesterålen archipelago and the Scandinavian mainland, and is characterized by Precambrian bedrock overprinted by the northern Scandinavian Caledonides. The origin of the high topography in the Caledonian mountain range, and particularly that of the Lofoten and Vesterålen islands, is a matter of debate. Proposed mechanisms include isostatic support from within the crust and lithosphere, elastic effects, dynamic topography, as well as isostatic contributions from glacial erosion (e.g., Breivik et al., 2020; Ebbing & Olesen, 2005; Gradmann et al., 2017; Maystrenko et al., 2020; Medvedev & Hartz, 2015; Nielsen et al., 2009; Schermer et al., 2017).

Several complementary geophysical datasets are available in the region, such as gravity, magnetics, active and passive seismics. However, interpretations of these datasets show considerable differences that have led to a debate concerning the structure and isostatic state of the lithosphere. An underlying objective of this study is to reconcile the different observations into a uniform structural and isostatic framework of the region. The solution may lie in the conceptualization of the Moho as a complex structure that marks the crust-mantle transition and is defined by multiple layers and/or gradients in *Vp*, *Vs* and density.

We use teleseismic data from available broadband stations in the study area and perform a receiver function (RF) inversion to quantify the crustal and upper mantle velocity structure. The advantage of our approach is that receiver functions have a good vertical resolution and that we are treating the entire data set from 62 stations with the same methodology and selection criteria. Previous RF estimates were based on H-κ stacking (Ben Mansour et al., 2018; Zhu & Kanamori, 2000), which by itself treats the crust as a single layer and does not account for intra-crustal complexities, such as HVLC and gradients. Our new results add important structural constraints to the discussion from an independent, complementary seismological method that provides new insight into the fine layering of the crust and upper mantle. We compare our results with three published crustal models (Ben Mansour et al., 2018; Maystrenko et al., 2017; Shiddiqi et al., 2022), as well as local refraction seismic lines and discuss implications for the controversial topics of crustal thickness, the nature of the crust-mantle transition and the state of isostasy in the Nordland and Troms region.

2. Background

2.1. Tectonic Setting

The surface geology in Nordland and Troms comprises the Caledonian Upper and Uppermost Allochthons, which were thrust on top of Precambrian Baltican basement during the Silurian-Devonian Caledonian orogeny (e.g., Froitzheim et al., 2016; Gee, 2015; Roberts, 2003; Steltenpohl et al., 2011). After initial post-orogenic extension of the Caledonides in the Devonian (Fossen, 2010; Osmundsen & Ebbing, 2008), continental rifting formed deep sedimentary basins in the Permian-Triassic to Cenozoic (Færseth, 2012; Gernigon et al., 2020; Schiffer et al., 2020). Rifting in the present-day Lofoten-Vesterålen continental margin (LVCM) culminated in continental breakup in the early Eocene, likely as one of the earliest segments forming the Northeast Atlantic Ocean (e.g., Bergh et al., 2007; Gernigon et al., 2020; Hansen et al., 2011). The LVCM is bound by the Senja Fracture zone to the north and is separated from the Vøring margin to the south by the Bivrost lineament (Blystad, 1995; Doré et al., 1997; Gernigon et al., 2020; Olesen et al., 2002).

The Baltican Archean-Palaeoproterozoic basement and Mesoproterozoic batholiths of the Transscandinavian Igneous Belt underlying the Caledonian allochthons are locally exposed in basement windows (Koistinen et al., 2001). Eclogites derived from continental lower crust of Baltica can be found in the Lofoten archipelago, bearing witness to subduction, metamorphism and exhumation of the Baltican lithosphere during the

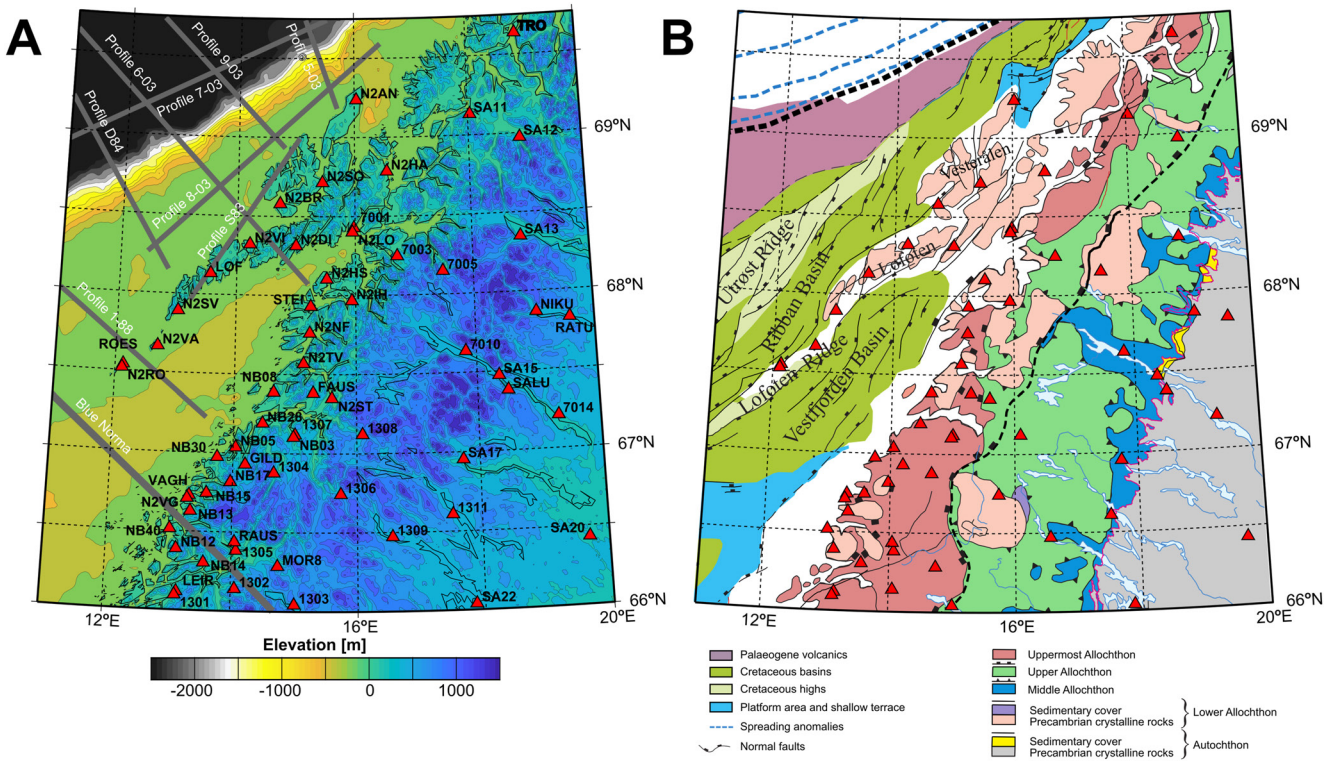

Figure 1. Physiographic and tectonic setting of Nordland and Troms. (a) Elevation (Amante & Eakins, 2009), stations (red triangles) and station names. (b) Geological-Tectonic map after (Mosar et al., 2002) with station locations (red triangles). Gray lines show approximate locations of refraction seismic lines: Profiles 6-03 (Breivik et al., 2017), 7-03, 8-03 (Breivik et al., 2020), 5-03 and 9-03 (Tsikalas et al., 2005), S83 (Sellevoll, 1983), D84 (Drivenes et al., 1984), 1–88 (Mjelde et al., 1993), Blue Norma (Theilen & Meissner, 1979).

Caledonian orogeny (Froitzheim et al., 2016). The region is crosscut by the NNW-SSE oriented Precambrian Bothnia-Senja-Kvænangen Fault Complexes in the north (Talbot, 2001), which have likely contributed to the structural evolution and compartmentalization of the LVCM including the Senja Fracture Zone (Gernigon et al., 2020; Schiffer et al., 2020).

The LVCM was structurally inverted during multiple phases in the Cenozoic (Doré & Lundin, 1996; Færseth, 2012; Stephenson et al., 2020). The complex landscape in Nordland and Troms was finally modified by Quaternary glacial erosion creating deep fjords and stripped mountain ranges. While erosion would generally result in overall decrease of the topography in the region, preserved summits separating the deeply carved fjords may have been experiencing net uplift (Medvedev & Hartz, 2015; Olesen et al., 2013). Apatite Fission track ages in the Lofoten Vesterålen archipelago are anomalously young compared to most of Scandinavia, which may be due to very recent (Palaeogene) and even present-day tectonic activity (Bergh et al., 2007; Osmundsen et al., 2010), potentially related to the vicinity of the rifted continental margin (Medvedev & Hartz, 2015). Kierulf et al. (2021)'s GNSS-derived model indicates that the Lofoten archipelago is currently subsiding by up to 0.8 mm/yr while the onshore areas experience uplift of up to 0.8 mm/yr due to tectonic or erosion processes.

Today, the structurally outstanding Lofoten-Vesterålen archipelago and its southern, mostly sub-marine extension, the Lofoten Ridge, form a coast-parallel geomorphologic high, separated from the Scandinavian mainland by the Vestfjorden Basin (Figure 1).

2.2. Crustal Structure of Nordland and Troms

The crustal structure of the LVCM was extensively studied by refraction seismic surveys, primarily offshore (see Breivik et al., 2020 and Maystrenko et al., 2020 for full overview), as well as by 2D and 3D potential field studies (Gradmann & Ebbing, 2015; Maystrenko et al., 2017; Olesen et al., 2002; Reynisson et al., 2010; Tsikalas et al., 2005). During the last decades, a growing number of temporary seismological networks and the expansion

of permanent seismological networks have provided the basis for more detailed studies of the crustal structure onshore, exemplified by recent RF (Ben Mansour et al., 2018) and local earthquake tomography (Shiddiqi et al., 2022) studies. Despite the comprehensive and diverse geophysical data coverage in the region, disagreement still exists about the depth and nature of the crust-mantle transition, the isostatic state of the lithosphere and the reason for high topography (e.g., Breivik et al., 2020; Maystrenko et al., 2020).

The LVCM is crossed by at least six coast-perpendicular (Avedik et al., 1984; Breivik et al., 2017; Drivenes et al., 1984; Goldschmidt-Rokita et al., 1988; Mjelde et al., 1993, 2003) and two coast-parallel crustal-scale seismic refraction lines (Breivik et al., 2020; Sellevoll, 1983), some of which cover the Lofoten-Vesterålen archipelago. The Moho depth model of Maystrenko et al. (2017; Figure 2a) is a good representation of the refraction seismic Moho estimates, as these were used as a tight constraint for the gravity modeling. The Lofoten-Vesterålen shelf south of the Lofoten-Vesterålen archipelago (~68°N) is ~250 km wide and has a Moho depth of typically 22–25 km (Avedik et al., 1984; Drivenes et al., 1984; Goldschmidt-Rokita et al., 1988; Mjelde et al., 1993, 2003). Here, the Lofoten Ridge represents a local anomaly with a minimum in crustal thickness of ~22 km and a considerably higher bathymetry and bedrock topography than on the surrounding shelf. The Moho beneath the central Lofoten-Vesterålen archipelago is up to ~36 km deep (Breivik et al., 2017) and the shelf narrows to ~50–100 km, forming an abrupt transition between the continental crust of the central Lofoten and the oceanic domain to the northwest (Breivik et al., 2017, 2020). An early seismic line crossing the Lofoten islands (Sellevoll, 1983) is not considered here due to large mismatches with modern datasets, possibly caused by differences in data quality and processing workflow, as described by Breivik et al. (2017). HVLC is primarily observed along the continent-ocean transition of the LVCM, as well as offshore the Lofoten-Vesterålen seaboard in a more proximal location on the margin (Breivik et al., 2017, 2020; Maystrenko et al., 2017).

Historically, the crust of the north-western Scandinavian mainland has not been as extensively investigated as its offshore counterpart. A single refraction seismic line crossing the Nordland and Troms area was acquired in the 1970s (BLUE NORMA), indicating a Moho depth of ~40 km (Avedik et al., 1984; Theilen & Meissner, 1979). A large magnetotelluric survey across Northern Norway and Sweden, including Nordland and Troms and the Lofoten-Vesterålen archipelago, shows the presence of an upper-crustal conductive anomaly beneath Nordland (Cherevatova et al., 2015), possibly related to the presence of water. Until recently, only sparse information from the permanent seismic networks was available, indicating a Moho depth of ~40 km at station TRO (Ottemöller & Midzi, 2003). Today, data from more than 60 stations from the Norwegian (Ottemöller et al., 2018) and Swedish (Lund et al., 2021) national seismic networks, as well as a series of temporary networks (SCANARRAY, Thybo et al., 2021; NEONOR2, Michálek et al., 2018; SCANLIPS-2 and -3D, Ben Mansour et al., 2018) are available for seismological studies in the onshore portion of Nordland and Troms. However, only parts of this new comprehensive data set have been so-far analyzed with RF techniques to provide information about the crustal structure of the Scandinavian mainland (Ben Mansour et al., 2018; Ottemöller & Midzi, 2003). These studies indicate Moho depths between ~40 and ~48 km in the onshore domain.

Three geophysical models describing the region's crustal structure are used in this study as a basis for comparison (Figure 2). First, there is a gravity model by Maystrenko et al. (2017), shown in Figure 2a, which is based on prior information from seismic refraction models crossing the region and covers almost the entire study area (with the exception of 2 stations). Second, there is a local earthquake tomography model which uses a comprehensive seismological data set and covers both the onshore and offshore domains of the region from ~66°N to 69°N (Shiddiqi et al., 2022; Figure 2b). Third, we produce a Moho depth compilation (Figure 2c) based on published RF inversion and H-κ stacking results from stations mainly distributed on the mainland (Ben Mansour et al., 2018; Olsson et al., 2008; Ottemöller & Midzi, 2003; Silvennoinen et al., 2014), similar to the composite map previously shown by Ben Mansour et al. (2018). To generate the compilation map of Figure 2c, we interpolated between the individual station results, smoothed the mapped values over a running averaging window of 15 km radius, and displayed the model in areas with a maximum radius of 25 km around every station used. A visual comparison of the panels in Figure 2 reveals that the overall trends in Moho depth between the three models are very similar, but obviously with local differences. A detailed comparison of these models, as well as the newly produced model, will be provided in Section 4.1.

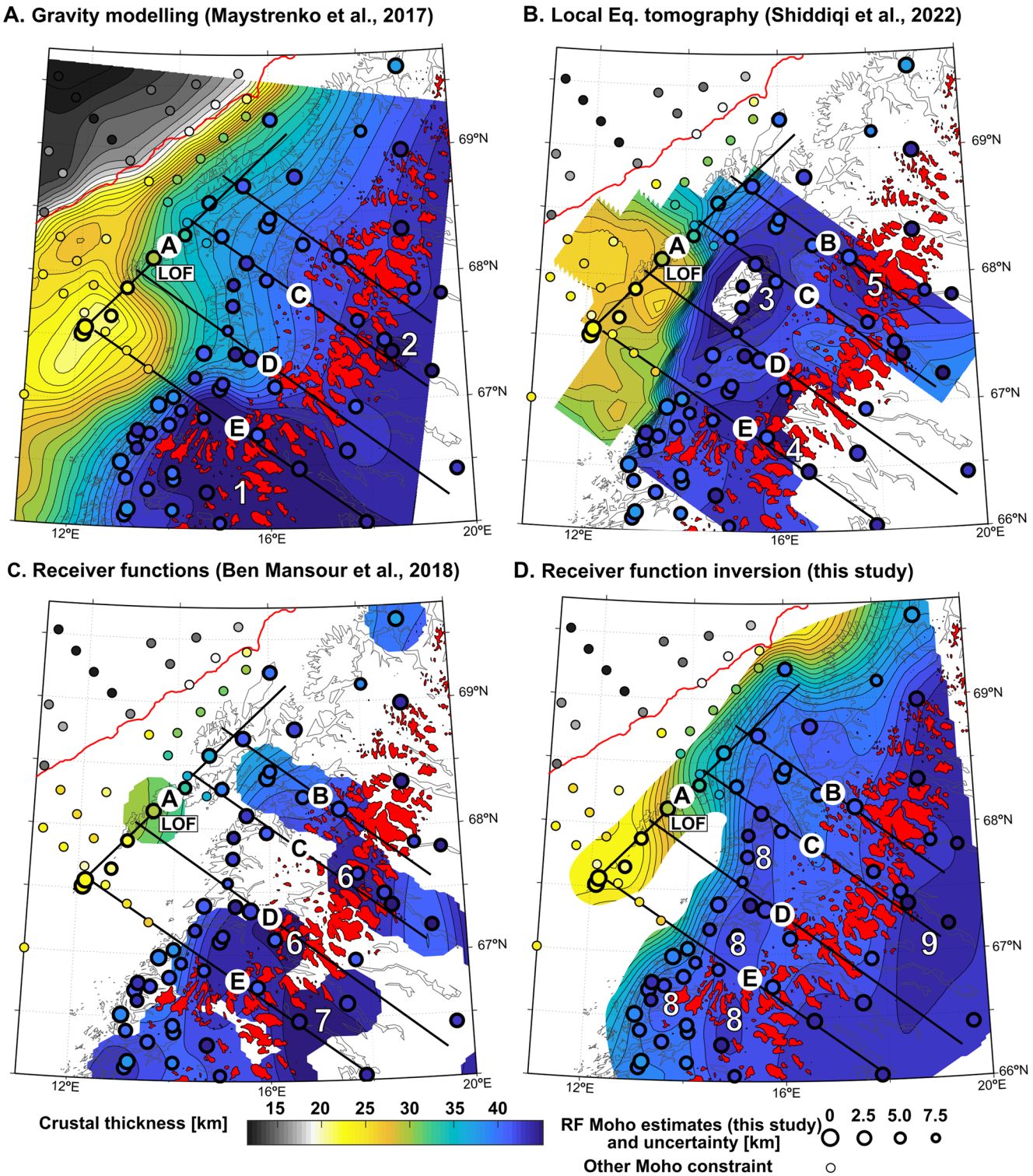

Figure 2. Moho depth models for the Nordland and Troms area (a–d) show various published Moho models (a) Maystrenko et al. (2017), (b) Shiddiqi et al. (2022) and (c) Combined RF estimates from Ben Mansour et al. (2018), Ottemöller and Midzi (2003), Olsson et al. (2008) and Silvennoinen et al. (2014). Large circles are the station-wise Moho depth estimates from this study as comparison. The size of the circles indicates the Moho uncertainty (large—small uncertainty; small—large uncertainty) (a) Moho depth model from interpolated and smoothed RF inversion results (this study) with additional constraints from refraction seismic lines (Breivik et al., 2017, 2020; Drivenes et al., 1984; Goldschmidt-Rokita et al., 1988; Mjelde et al., 1993) and gravity inversion profiles (Tsikalas et al., 2005) closest to the seismometers used for RF inversion. Cross sections A-E are shown in Figure 4. Red areas show topography higher than 1,500 m.

2.3. Isostatic State of the Lofoten-Vesterålen Archipelago

There is an ongoing debate concerning the isostatic state of the Lofoten-Vesterålen archipelago and the Lofoten Ridge. This debate is rooted in two attributes: (a) the high topography of the Lofoten Ridge, which is inconsistent with the apparent thin crust (Breivik et al., 2020; Gradmann et al., 2017; Maystrenko et al., 2017, 2020; Tsikalas et al., 2005); and (b) the high gravity anomaly of >100 mGal associated with the Lofoten-Vesterålen archipelago (Reynisson et al., 2010; Tsikalas et al., 2005). Tsikalas et al. (2005) found that the Moho architecture alone cannot explain this gravity anomaly and proposed the existence of high-density structures in the crust of the Lofoten Ridge and southern Lofoten Islands to explain the missing ∼50 mGal. This is in contrast to the central-northern Lofoten-Vesterålen archipelago where these high crustal densities are not required and at the same time the crust is ∼10–15 km thicker, suggesting a major change in crustal structure and properties (Tsikalas et al., 2005). Reynisson et al. (2010) came to a similar conclusion that there are large differences in Moho depth suggested by isostatic and gravity models beneath the southern Lofoten and Lofoten Ridge. In their regional analysis, Ebbing and Olesen (2005) observe a clear positive isostatic gravity anomaly along the southern Lofoten and the Lofoten Ridge. This anomaly indicates that the crust here is not in crustal isostatic equilibrium and the topography too high if one simply assumes a constant crust-mantle density contrast of 350 kg/m^3. Mjelde et al. (2013) proposed that the shallow Moho interpretation beneath the Lofoten Ridge may reflect the top of a lower crustal eclogite body, similar to interpretations in other parts of the Norwegian margin, implying a greater actual Moho depth (from a petrological point of view). This argument was recently renewed by Breivik et al. (2020). In contrast, the recent regional density model of the LVCM by Maystrenko et al. (2017) used a shallow Moho along the southern Lofoten and Lofoten Ridge, based on the original seismic images by Mjelde et al. (1993) with a high-density crustal layer to fit the local high gravity anomaly. Additionally, they employed a mantle lithosphere beneath the Lofoten Ridge and the northern LVCM that is ∼20–35 kg/m^3 less dense than the surrounding mantle lithosphere.

The overarching problem is well-illustrated by the modeling results of Gradmann et al. (2017), who find that the shallow Moho and excess mass needed to fit the gravity anomaly are inconsistent with the high topography of southern Lofoten. Earlier observations of Gradmann and Ebbing (2015) that the peaks of free air anomaly, Bouguer anomaly, and high topography in the study area do not coincide with another, preclude a simple crustal isostatic framework. The Lofoten-Vesterålen archipelago was deformed and experienced vertical motions since at least the Palaeogene, likely related to continental breakup processes, and still experiences active tectonic deformation today (Bergh et al., 2007; Osmundsen et al., 2010).

3. Data and Methods

To help resolve the disagreement about crustal structure and isostasy across Nordland and Troms, we develop a new, complementary crustal model based on receiver function inversion of the available stations in the region.

3.1. Receiver Function Analysis of Teleseismic Data

We investigate the crustal and upper mantle structure of the Nordland and Troms area by means of inversion of RFs and P-wave polarizations, which are two data products derived from raw teleseismic waves recorded at three-component broadband seismometers. RFs have a good vertical resolution, but when handled individually, information on absolute velocity variations is not well-constrained. We therefore employ P-wave polarizations as an additional data set, from which we can first derive and then invert S-wave velocities Vs_{app} (Svenningsen & Jacobsen, 2007).

The raw three-component teleseismic data for RF and Vs_{app} processing are extracted from 62 stations that are part of the Norwegian National Seismic Network (NNSN, Ottemöller et al., 2018, network code NS), the Swedish National Seismic Network (SNSN, Lund et al., 2021, UP) and the temporary networks ScanArray (Thybo et al., 2012, 1G), NEONOR2 (Michálek et al., 2018), SCANLIPS2 and SCANLIPS3D (Ben Mansour et al., 2018; England, 2013; Y1, ZR).

Our first data product, the receiver function (RF), provides an estimate of the Earth's impulse response beneath a station by deconvolving the incident P-wavefield of teleseismic earthquakes from the P-to-S (Ps) converted wavefield (e.g., Langston, 1979; Vinnik, 1977). Deconvolution equalizes source and path effects, as well as the instrument response, to represent the Ps conversions as isolated pulses in the coda of the direct P-arrival (e.g.,

Ammon, 1991; Clayton & Wiggins, 1976; Langston, 1979; Ligorría & Ammon, 1999; Vinnik, 1977). An RF is composed of the superimposed primary conversions (Ps) from every velocity discontinuity, as well as conversions from free-surface multiples including one P-s conversion (so-called PpPs and PpSs) and two P-s conversions (so-called PsPs)—see, for example, Zhu and Kanamori (2000). In multi-layer models, the conversions from shallower layers may overprint and disturb the primary conversions from greater depths. The raw data were all processed following the automated workflow developed for the global RF database "Global Imaging using Earthquake Records" (GLImER; Rondenay et al., 2017). This workflow includes the rotation of traces into the R-T-Z (radial-transverse-vertical) component system, filtering of the data between 0.03 and 1.5 Hz, data selection based on signal-to-noise ratio criteria on the vertical and horizontal components, and spectral domain deconvolution with a regularization parameter (pre-whitening term) based on the maximum of the amplitude spectrum of the pre-event noise (see Rondenay et al., 2017 for details). After automatic and manual quality control, our final data set consists of 3283 RF waveforms. This represents an average of 53 RFs per station, with a high station-to-station variability ranging from a minimum of 9 RFs to a maximum of 323 RFs. These differences stem from the type of instrument used, the noise environment at the station location, as well as the duration of deployment.

Our second data product, the polarisation of incident teleseismic P-waves, provides information about the S-wave velocity distribution beneath a seismic station (Svenningsen & Jacobsen, 2007). This information is retrieved from the ratio of the radial (R) to the vertical (Z) RFs at zero delay time of the RFs (Svenningsen & Jacobsen, 2007). The obtained velocities are apparent velocities (Vs_{app}) of the integrated vertical structure sampled by the dominant wavelength of the incident wave. Using increasing wavelengths of the incident waveform, we can compute successive values of Vs_{app} that capture greater depths. This set of Vs_{app} values can then be inverted to obtain a model of absolute velocity versus depth beneath the seismic station. Here, we produce curves of Vs_{app} at increasing periods (T), following the procedure by Svenningsen and Jacobsen (2007). The periods are defined as 51 values logarithmically scaled from 1 to 25 s.

We find that most stations yield physically meaningful RF waveforms and P-polarizations, with the exception of station LOF. At LOF, the average horizontal component exhibits very low amplitudes near tPs = 0 s, where one expects to see some energy of the direct P-arrival. This low average amplitude of ∼0.2, with some amplitudes below 0.1, translates into an extremely low Vs of ∼1.5 km/s, which we consider as unrealistic, considering that station LOF is located on bedrock. We therefore double the uncertainty of Vs_{app} at this station. The increased data uncertainty will automatically increase the weight on the RF waveform and a priori model constraints, and will translate into a larger model uncertainty (see Section 3.2).

3.2. Joint Inversion

To obtain 1D velocity models of the crust and upper mantle beneath each individual station, we jointly invert the two sets of teleseismic data products (RF and polarisation). We employ a slightly modified version of the inverse algorithm by Schiffer et al. (2022), which itself is based on earlier versions that were successfully applied to other datasets (e.g., Schiffer et al., 2019).

Our approach combines a linearized iterative least squares (LLSQ) inversion (Ammon et al., 1990; Menke, 1989; Tarantola & Valette, 1982) with a random model search scheme. For every station, we calculate 1,000 full LLSQ inversion runs and save the last 10 iterations, to provide a statistically large enough posterior model distribution of 10,000 models. Each inversion runs for at least 15 iterations and a maximum of 50 iterations. The minimum of 15 iterations was chosen such that we can always save the last 10 models of the inversion while still allowing for fast conversion over the first five iterations. We deem that if the inversion has not converged after 50 iterations, the problem may be ill-posed, and we end the individual inversion. We use highly variable, randomly generated starting models that satisfy the following conditions: (a) The S-wave velocities are limited to a range between 2 and 5 km/s and must be monotonously increasing with depth; (b) Each model has between 5 and 20 layers; (c) the lowest half-space velocity must not be less than 4.5 km/s; (d) a random fraction of the layer boundaries is defined at the observed peaks in the RFs between 1 and 6 s; and (e) the maximum model depth is 80 km.

The stacked RFs are modeled from −1 to 25 s delay time and the median Vs_{app} curves are computed for periods from 1 to 25 s, with both ranges corresponding to depths of approximately 0–200 km. *A priori* data errors are based on the data covariance matrices and automatically weigh the two data sets.

We primarily model *Vs* and the thickness of each layer, and couple *Vs* to a *Vp*/*Vs* ratio lookup table based on typical lithologies (Christensen, 1996) to also obtain a corresponding *Vp* (see Schiffer et al., 2022 for details). Furthermore, we can constrain densities from *Vp* using a depth-dependent relationship (Christensen & Mooney, 1995). The non-uniqueness of the inverse problem is reduced by parameterizing layers in delay-time instead of thickness (Jacobsen & Svenningsen, 2008). During the inversion, velocities and depths/delay times are virtually unconstrained in the inversion and can freely change without causing any significant model error, with the exception of the lowermost, half-space velocity, which is assigned an a priori model error of 0.2 km/s, forcing the lowermost velocity to settle around typical mantle velocities.

Each inversion yields an a posteriori data and model error (*Qd* and *Qm*) defined as the root mean square errors relative to the observed data and starting model, weighted with the prior uncertainties. An additional model roughness error (*Qr*) is defined by the second derivative of the velocity model. The total error *Q* is defined as the sum of these error terms (see Schiffer et al., 2016 for details). Each inversion is terminated when the total error converges (i.e., two consecutive changes of less than 0.1%), or at a maximum of 50 iterations. The 10,000 models weighted with their inverse *Q* form a posterior model population. If the inverse problem is not ill-posed, the data have little noise, and the underlying geology is simple, typically the inversion converges quickly, so that the last 10 iterations should be very similar, with a small spread and corresponding model uncertainty. Conversely, an ill-posed inverse problem, noisy data, and complex underlying geology may result in ineffective convergence, in which case the last 10 iterations may be much more broadly distributed, translating to a larger model uncertainty compared to the former case. Similarly, if the a priori data error is large, the inversion will find models with a larger spread as it does not attempt to fit the data too tightly, and this will result in larger model uncertainties. In the case of station LOF, where the a priori error of Vs_{app} was doubled, more weight is automatically given to the receiver function data and to the other error terms (*Qm* and *Qr*; though note that *Qm* is negligible since the starting model is almost virtually unconstrained).

4. Results

The results at the individual stations are used to generate a regional model of Moho depths. We interpolate between the individual Moho depth estimates and smooth the map along a running window with radius of 15 km, which roughly corresponds to the area at Moho depth covered by the incoming teleseismic waves beneath a station (e.g., Rondenay, 2009). The final model is presented in map view in Figure 2d and cross-sections are shown in Figure 4. In the following we describe our model and draw comparisons with other crustal models, first in the "offshore domain", including the Lofoten-Vesterålen archipelago followed by the onshore domain.

In the offshore domain, including the Lofoten-Vesterålen archipelago, our results suggest an extremely shallow Moho along the Lofoten Ridge and southernmost Lofoten archipelago, with a sharp Moho step in the central Lofoten at approximately 68.0°N, between stations LOF and N2SV (Figures 2d and Figure 4). In comparison, the tomography shows the step slightly further north (~68.3°N) while the gravity model places it on the southern tip of the Lofoten islands (~67.9°N). The only previous result from RF analysis suggests ~30 km Moho depth at LOF (Ottemöller & Midzi, 2003). The shallow Moho of <25 km to the south is very similar to what was observed in the active source seismics by Goldschmidt-Rokita et al. (1988) and Mjelde et al. (1993), and is confirmed by gravity modeling (Maystrenko et al., 2017). The local tomography in the same area suggests a ~5 km deeper Moho, but places the shallowest Moho of 25 km to the west (Vestfjorden Basin) and east (Lofoten shelf) of the southern Lofoten islands. The RF model does not have sensitivity between the available stations, hence, the Moho depth in the Vestfjorden basin is unknown (Figure 2d). Currently, the local earthquake tomography of Shiddiqi et al. (2022) is the only model that provides direct constraints on Moho depth in the Vestfjorden Basin. The Moho depth in the northern Lofoten and Vesterålen is generally consistent for all models, although the RF inversion suggests a slightly deeper Moho in northernmost Vesterålen. Interestingly, the top of the HVLC interpreted from RFs (see next sub-section) coincides almost exactly with the Moho depth from gravity modeling (Figure 4).

On the Scandinavian mainland, the Moho depth typically ranges between ~37-47 km in all four models, but with distinct local differences (Figures 2a and Figure 5). The gravity model (Figures 2a, Maystrenko et al., 2017) displays very deep Moho of >45 km south of ~67°N (feature 1) and >42 km at the eastern edge of the study area (feature 2). In coast-near areas north of ~67°N, shallower Moho in the range of ~35–40 km depth is observed. Earthquake tomography (Figure 2b, Shiddiqi et al., 2022) suggests three areas of deep Moho: one very deep Moho anomaly on the coastline of the mainland east of Lofoten (feature 3, 15°E, 68°N), another at the southeastern edge

of the model (feature 4, 16°E, 67°N) and the last at the northeastern edge of the model (feature 5, 18°E, 68°N). The compiled RF model (Figures 2c and Ben Mansour et al., 2018) suggests a large Moho depth of ∼42–43 km in the south-central part of the study area (features 6 and 7), partly overlapping with regions of deep Moho in the earthquake tomography (feature 4) and the gravity model (feature 8). Their RF model also suggests deep Moho of >42 km at the eastern edge of the study area, similar to the gravity model. By comparison, our model shows a consistently deep Moho (∼40–42 km) along the Norwegian coastline (feature 8), and the Moho appears to be shallower (∼37–40 km) further inland where the topography is highest (Figure 2d). While the background Moho depths from our model are similar to those from the tomographic model, the RFs do not recover the two deep Moho anomalies (features 3 and 6). Similarly, the deep Moho in the gravity model (feature 1) and previous RF model (features 6 and 7) could not be recovered by this study. However, the increasing Moho depth at the eastern edge of the study area is consistent with the gravity model. The gravity and local tomography models show a considerable Moho step between onshore and offshore domains that follows roughly the coastline. In both models, this step marks an abrupt westward shallowing of the Moho from ∼40 to 45 km depth beneath the Scandinavian mainland to ∼25–30 km depth beneath the LVCM. However, the sharpness and exact location of this step varies between the two models (Figure 2). The feature that is least consistent between all three models is a zone of Moho depth >45 km (feature 3 in Figure 2b), which is only observed in the earthquake tomography.

Comparison of the Moho depth estimates of the four models at the station locations used in this study (Figure 5) shows that our model is most consistent with the previous RF study (root mean square difference of 1.9 km), which also has the smallest overlap with the study area. The earthquake tomography and gravity models show more substantial differences (root mean square difference of 2.7 km for both). Comparison of Moho depth estimates in the Lofoten-Vesterålen archipelago (Figure 5, red circles) shows that the shallowest Moho depth estimates on the Lofoten Ridge (<30 km) seem to best match the gravity model, while the tomography exhibits up to ∼3–5.5 km deeper Moho. The estimates at the near-coast stations (Uppermost Allochthon, purple circles) and the areas of highest topography (Upper Allochthon, green circles) are more consistent with the H-κ RF model and the tomography, but with usually slightly shallower Moho in our model. In the Middle Allochthon and the Precambrian shield (blue circles) our model shows similar differences to all three models.

The average Moho depth of our model is shallower than that of the other three models, with the largest difference to the tomography (1.37 km), followed by the previous RF model (0.97 km) and lastly the gravity model (0.09 km). Such differences could indicate systematic, methodological differences, or different behaviors of density, *Vp* or *Vs* across the Moho. This will be further addressed in Section 5.1.

4.1. High Velocity Lower Crust and Crust-Mantle Transition

Similar to the Moho depth map, we construct maps showing the thickness of HVLC, the uppermost mantle velocity (average velocity in an interval 0–5 km below the crust-mantle transition) and the velocity gradient of the crust-mantle transition, or Moho sharpness (Figure 7). These model elements characterize the nature of the crust-mantle transition as follows: (a) a combination of thin HVLC, high uppermost mantle velocity and large Moho velocity gradient indicate a sharp Moho discontinuity; and (b) vice versa, a combination of thick HVLC, low uppermost mantle velocity and low Moho velocity gradient describe a more complex crust-mantle transition. It can be challenging to properly distinguish between a HVLC layer and a gradual Moho, as these will have overlapping velocity ranges, so there likely is an inherent overlap between the two features (HVLC and crust-mantle transition). In our interpretation, the two features are formally defined as two separate structural elements without an overlap. Hence, there will be a trade-off between the thicknesses of HVLC and crust-mantle transition. Furthermore, the model elements describing the crust-mantle transition zone may not be as robust as the Moho depth itself, because their RF signal amplitude is typically lower and more easily overprinted by noise and multiples. To accommodate for these less robust individual quantities during the construction of the maps, we use a larger smoothing window with a radius of 25 km instead of the 15 km radius for the Moho depth model resulting in a more regional, smoother, but potentially more robust depiction of the results.

The RF model shows a clear regional variation in HVLC thickness (Figure 7a). There is a 4–8 km thick HVLC along the Lofoten-Vesterålen archipelago (Figure 3, feature I), which appears to branch out into a N-S oriented structure stretching from the central Lofoten to the southern bound of the study area (feature II, roughly along 15°E). This "southern branch" of thick HVLC coincides with a deeper Moho (Figure 6). Our model also indicates thicker HVLC along the eastern bound of the study area within the Fennoscandian shield (feature III, east

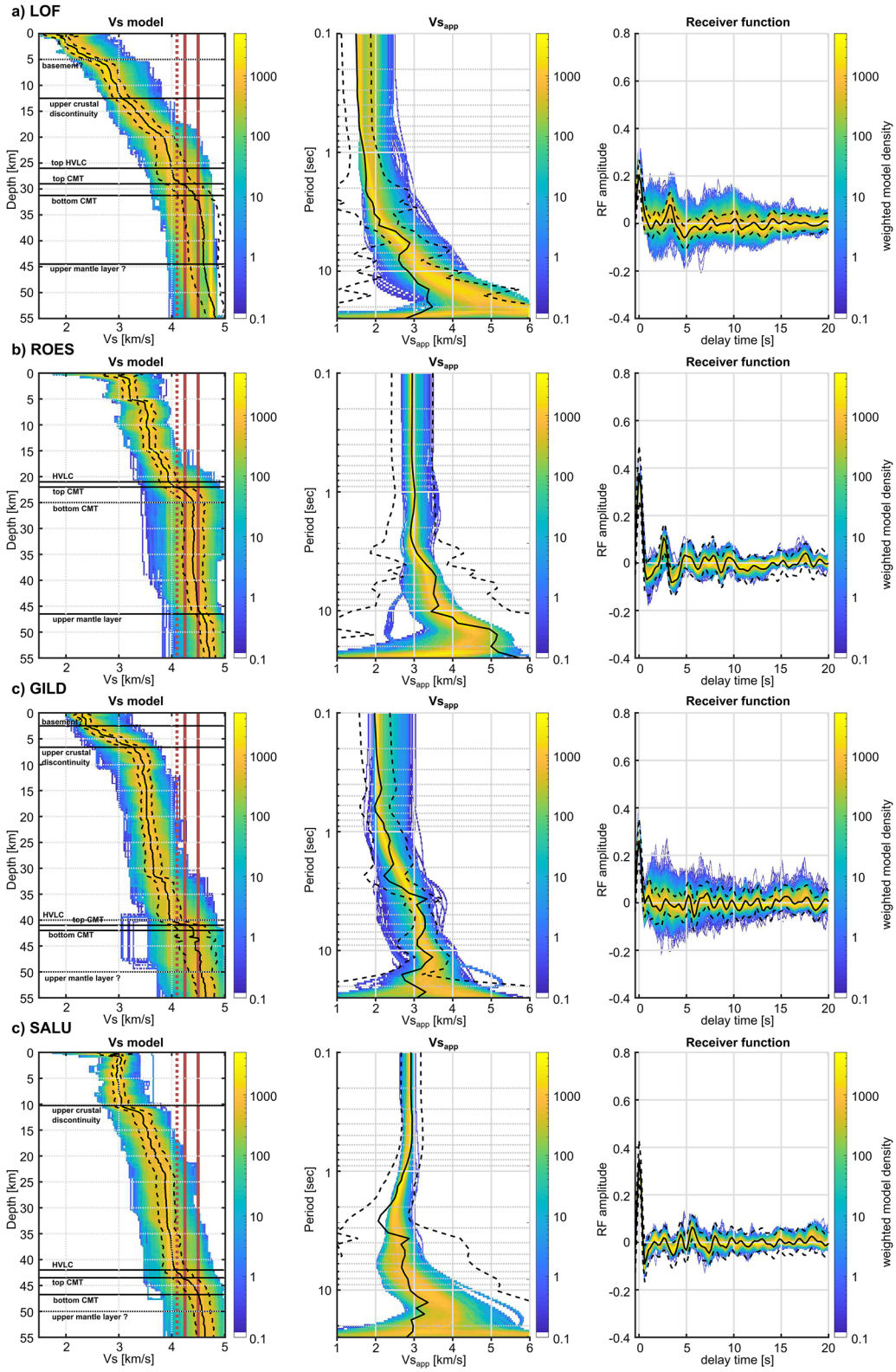

Figure 3.

of ∼18°E). Generally, we expect similar uncertainties and trade-offs for the HVLC thickness as for the Moho depth estimates.

Our HVLC estimates are generally consistent with the distribution and thicknesses of HVLC depicted in a map of the "lowermost high velocity crustal layer" (reprinted in Luosto, 1997). When compared to our results, the model published in the 1990s is based on P-wave wide-angle reflection-refraction data and has much lower spatial resolution, as it relies on the interpolation between fewer points and over a broader region. In that model, the area showing 4–8 km HVLC thickness coincides well with our observations for the mainland. However, the 1990s model shows no sign for increased HVLC in the Lofoten islands and some other details are missing. The "LCB" (high density lower crust) in Ebbing (2007)'s regional model over Fennoscandia shows LCB thicknesses of 0–5 km in the Lofoten-Vesterålen archipelago and 0–10 km on the mainland. However, except for a general eastward increase of LCB thickness, detailed anomalies and structures do not seem to match those observed in our model, which may be due to limited resolution of the regional-scale gravity-isostatic model of Ebbing (2007). Lastly, Maystrenko et al. (2017)'s model includes a high density lower crustal layer which agrees very well with the HVLC estimated by our inversion in the Lofoten-Vesterålen (features I), the south-striking feature (feature II), but also further inland.

The map of uppermost mantle velocity (average velocity in a 5-km interval below the base of the defined crust-mantle transition) (Figure 7b) clearly indicates lower velocities (4.3–4.5 km/s) along the coastline, particularly beneath the Lofoten-Vesterålen archipelago and the northern coastline of the study area (feature IV). The mainland away from the coast, with exception of one station in the south (feature V), is characterized by moderate uppermost mantle velocities (>4.5 km/s). Beneath the Lofoten-Vesterålen archipelago, we observe a sub-crustal discontinuity (Figure 4) that outlines a low-velocity layer in the uppermost mantle, directly below the Moho. The base of this uppermost mantle layer (UML) lies at a fairly constant depth of ∼45 km, causing the thickness of the UML to gradually decrease from ∼20 km beneath the Lofoten Ridge to less than 5 km beneath Vesterålen (Figure 4).

The velocity gradient of the crust-mantle transition, or Moho sharpness (Figure 7c), shows a very similar pattern as the HVLC thickness, which may not come as a surprise, as we often observe a HVLC in regions where the Moho gradient is small. We therefore use the same features as in Figure 7a to describe the distribution. The Lofoten-Vesterålen archipelago exhibits the lowest Moho gradient—or least sharp Moho—(feature I) and we can also observe a N-S trending anomaly reaching from the Lofoten islands to the south at ∼15°E (feature II), very similar to the corresponding HVLC structure. We also see a decreased Moho gradient along the eastern boundary of the study area, which again coincides with thicker HVLC (feature III).

4.2. Isostasy

We investigate the isostatic state of the crust in the Nordland and Troms area using two simple isostatic tests. In the first test, we compare topographic elevation-Moho depth relationships of the four regional crustal models (this RF study, gravity, tomography and previous RF studies) with theoretical Airy-isostatic relationships; in the second test, we investigate how the density of the low-velocity UML detected by our model affects the residual topography, also assuming local Airy-type isostasy.

1. We calculate predicted topographic elevation (h) by balancing homogeneous crustal columns with a given Moho depth (z) and crustal densities (ρ_c) of 2,600–2,900 kg/m^3 over a mantle with a density (ρ_m) of 3,300 kg/m^3, and where required the density of water (ρ_w) of 1,000 kg/m^3. Here, the z-axis points downwards, resulting in positive values for Moho depths. However, we define the topographic elevation (h) pointing

Figure 3. Inversion results for four example stations (a) LOF, (b) ROES, (c) GILD, (d) SALU showing the 10,000 posterior models weighted with their inverse data error. The color scale indicates the weighted model density (i.e., the sum of the inverse data error of all models covering a block; the integral over all velocities at every z are normalized by the number of models so that the sum of values at every depth interval is 10,000) Left: S-wave velocity models; center: Vs_{app} curves; right: RF waveforms. The final model is defined as the mean of the model population. The model uncertainty is defined as the 95% confidence interval of the model population. Horizontal black lines indicate major layer interpretations, such as the potential basement interface (in the study area probably representing the interface between metasedimentary layers and crystalline basement), the top of the high velocity lower crust (HVLC), and top and bottom of the crust-mantle transition (top/bottom CMT), if observed, as well as an interface in the upper mantle, if it was possible to identify such. The Moho is defined in the center of the crust-mantle transition. The vertical solid red lines indicate the typical range of the crust-mantle transition zone, the stippled vertical red line indicates the lower bound of typical velocities of HVLC, although these boundaries are not rigid in the interpretation and is only used as a guideline.

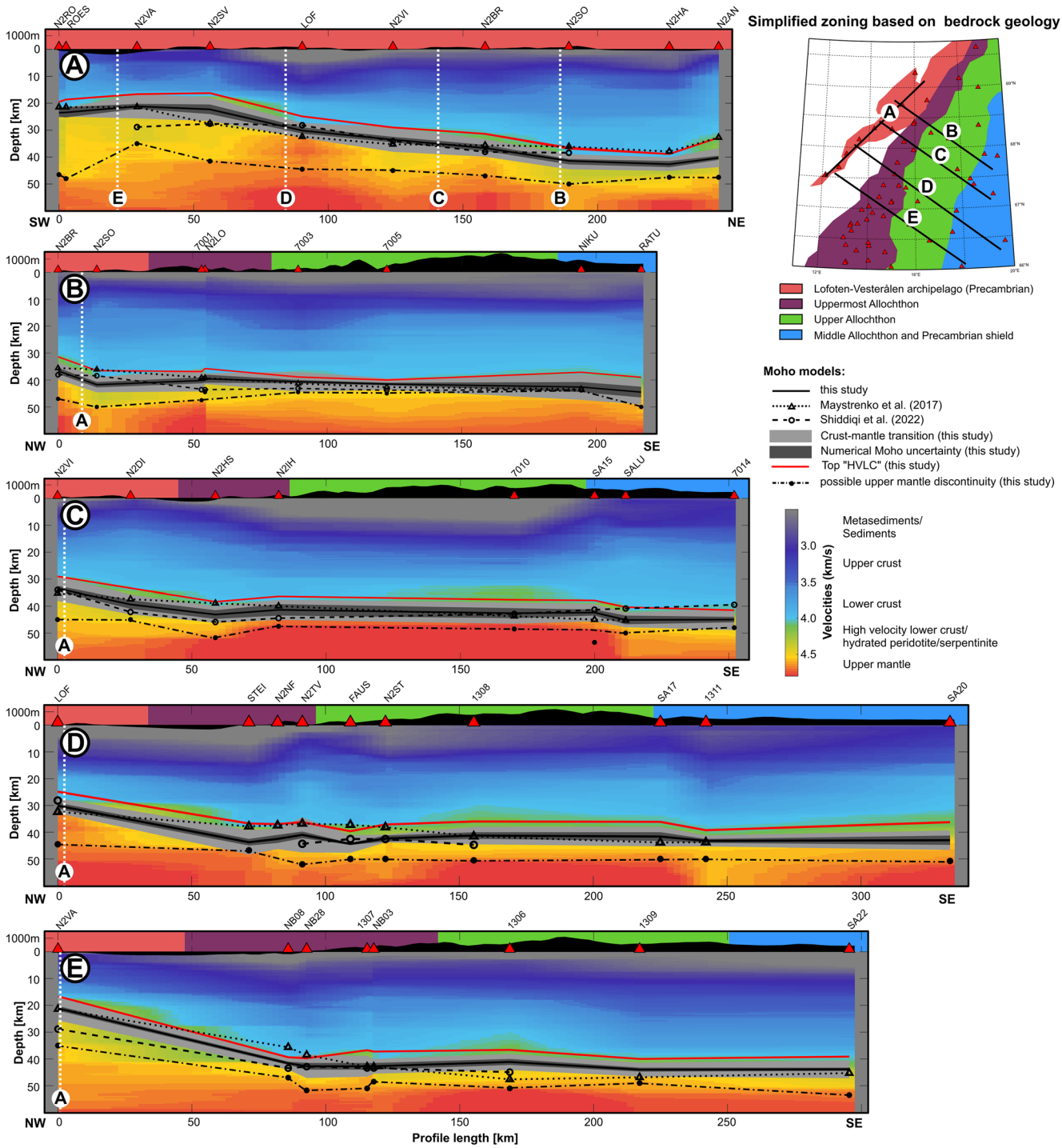

Figure 4. Cross sections through the study area (a–e) showing the laterally interpolated velocity model from RF inversion, the interpretation (Moho, high velocity lower crust—HVLC, and an upper mantle layer) and topography along the profiles averaged within a circular running window of 2.5 km radius with an exaggeration of factor 5 compared to the velocity structure. Approximate tectonic domains along each profile are represented by colored backgrounds. The model is compared to models from Shiddiqi et al. (2022) and Maystrenko et al. (2017), represented as hatched and stippled black lines, respectively. Locations of cross-sections are shown in the inlet and in Figure 2.

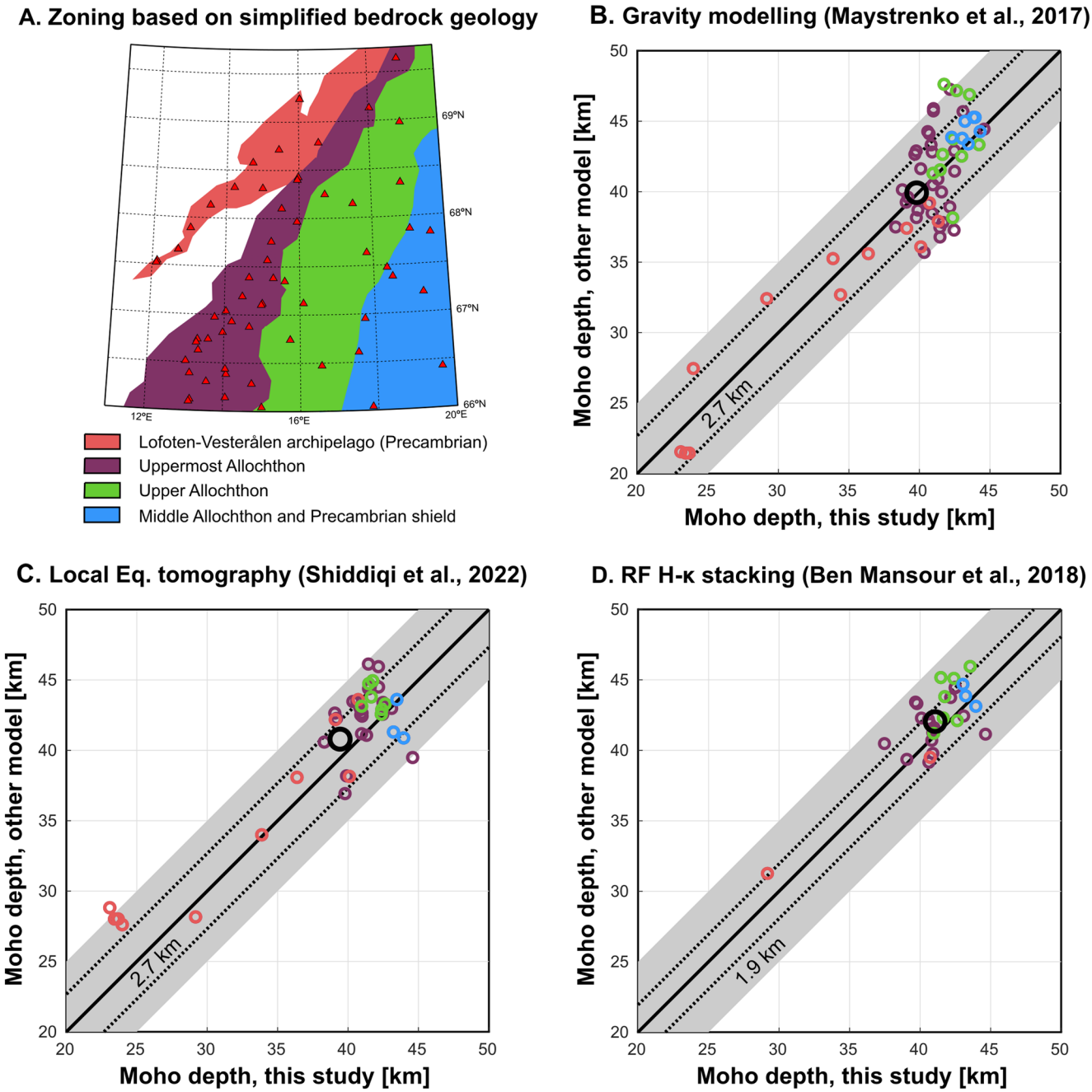

Figure 5. Comparison of different Moho depth models shown in Figure 2. Colored circles show average Moho depth values of an area with 10 km radius around every station used in this study. The larger, black circle shows the average of these Moho depth values. Comparisons are made with (b) the crustal gravity model (Maystrenko et al., 2017), (c) the crustal thickness model from local earthquake tomography (Shiddiqi et al., 2022) and (d) an earlier receiver function model (Ben Mansour et al., 2018). Colors indicate general zonation based on simplified bedrock geology (see Figure 6 for map): Red—Lofoten-Vesterålen archipelago; Purple—Coastal areas/Uppermost Allochthon; Green—Upper Allochthon; Blue—Middle Allochthon and Fennoscandian shield. Gray shading indicates a difference of 5 km between the respective models. Stippled black lines mark the root mean square difference between the two respective models.

upwards, resulting in positive values for onshore and negative values for offshore areas. We assume crustal compensation depths (z_{ref}) of 35 and 40 km and Airy isostasy. We then plot the observed topographic elevation and Moho depth readings of all four models and compare them with the theoretical trends (Figure 8). The theoretical trends are calculated by balancing a crust-mantle column with a reference crust-mantle column as follows, first for onshore regions:

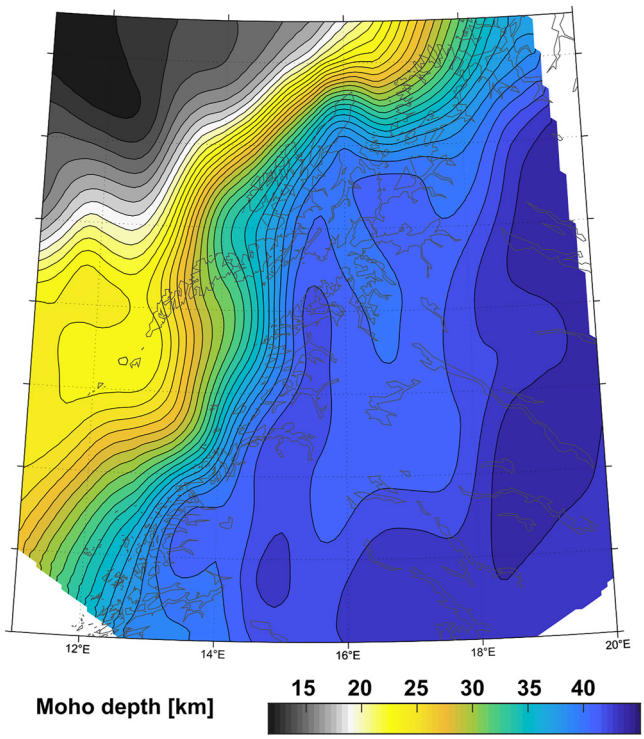

Figure 6. Moho depth from RF inversion with additional constraints from refraction seismic lines (Breivik et al., 2017, 2020; Drivenes et al., 1984; Goldschmidt-Rokita et al., 1988; Mjelde et al., 1993) and gravity inversion profiles (Tsikalas et al., 2005) closest to the seismometers used for RF inversion.

$$(h+z)\cdot\rho_c = z_{\text{ref}}\cdot\rho_c + (z-z_{\text{ref}})\cdot\rho_m\,; \quad z > z_{\text{ref}} \tag{1a}$$

$$h = (z-z_{\text{ref}}) * (\rho_m-\rho_c)/\rho_c\,; \quad z > z_{\text{ref}} \tag{1b}$$

and, second for offshore regions,

$$-h\cdot\rho_w + (z+h)\cdot\rho_c + (z_{\text{ref}}-z)\cdot\rho_m = z_{\text{ref}}\cdot\rho_c\,; \quad z < z_{\text{ref}} \tag{2a}$$

$$h = (z-z_{\text{ref}}) * (\rho_m-\rho_c)/(\rho_c-\rho_w)\,;\; z < z_{\text{ref}} \tag{2b}$$

These trends for the topographic elevation (Equations 1b and 2b) are simplified as they do not take into account possible variations in lithospheric structure, density and rheology or other isostatic effects. Nevertheless, the test is able to show whether and to what degree the region's topography may be explained by Moho depth changes, based on visual inspection.

For all crustal models, the stations along the Lofoten-Vesterålen archipelago (red) with crust <35 km show a large crustal thickness variation (>15 km), but only very minor topography variation (<100 m), implying that the topography here cannot simply be explained by crustal thickness variations. Crustal compensation could theoretically be achieved via density changes of ~300–500 kg/m^3 within the crust, but such large density variations seem unlikely. In areas away from the Lofoten Ridge, typically with crust >35 km, we observe rather different trends and patterns between the different models that usually (but not always) plot within the range of the tested theoretical trends. For our RF model (Figure 8d), a close-to-expected Airy-isostatic trend is observed using plausible reference densities and an apparent crustal compensation depth of ~40 km. However, there is a considerable scatter, in particular for the stations in the central Upper Allochthon, which follow a trend equivalent to slightly shallower compensation depths. Maystrenko et al. (2017)'s model (Figure 8a) follows a noticeably different trend on the mainland, with a slope that is much gentler than predicted by Airy-isostasy. Their density model includes lateral density changes in the crust and in the mantle lithosphere, which are not considered here. Most Moho depth estimates by Shiddiqi et al. (2022) (Figure 8b) on the mainland suggest crustal isostasy with a compensation depth of ~40 km. However, the very thick crust in the Uppermost

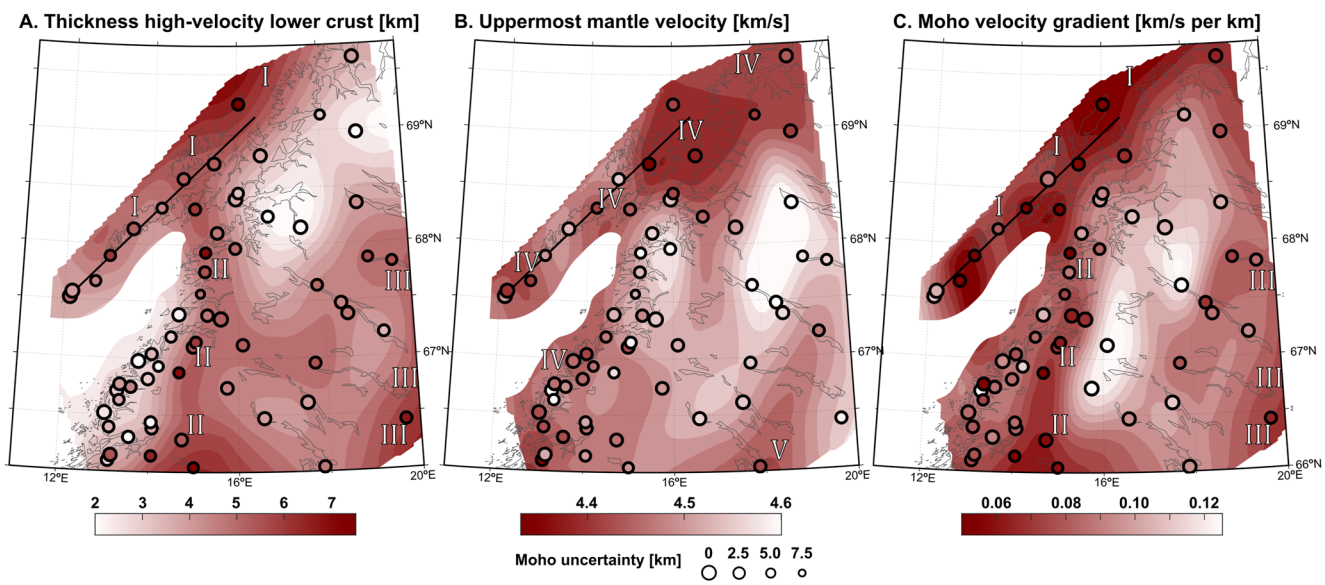

Figure 7. Nature of crust-mantle transition and the uppermost mantle: Thickness of the high velocity lower curst (HVLC) (a), upper mantle velocity (b) an Moho velocity gradient (c).

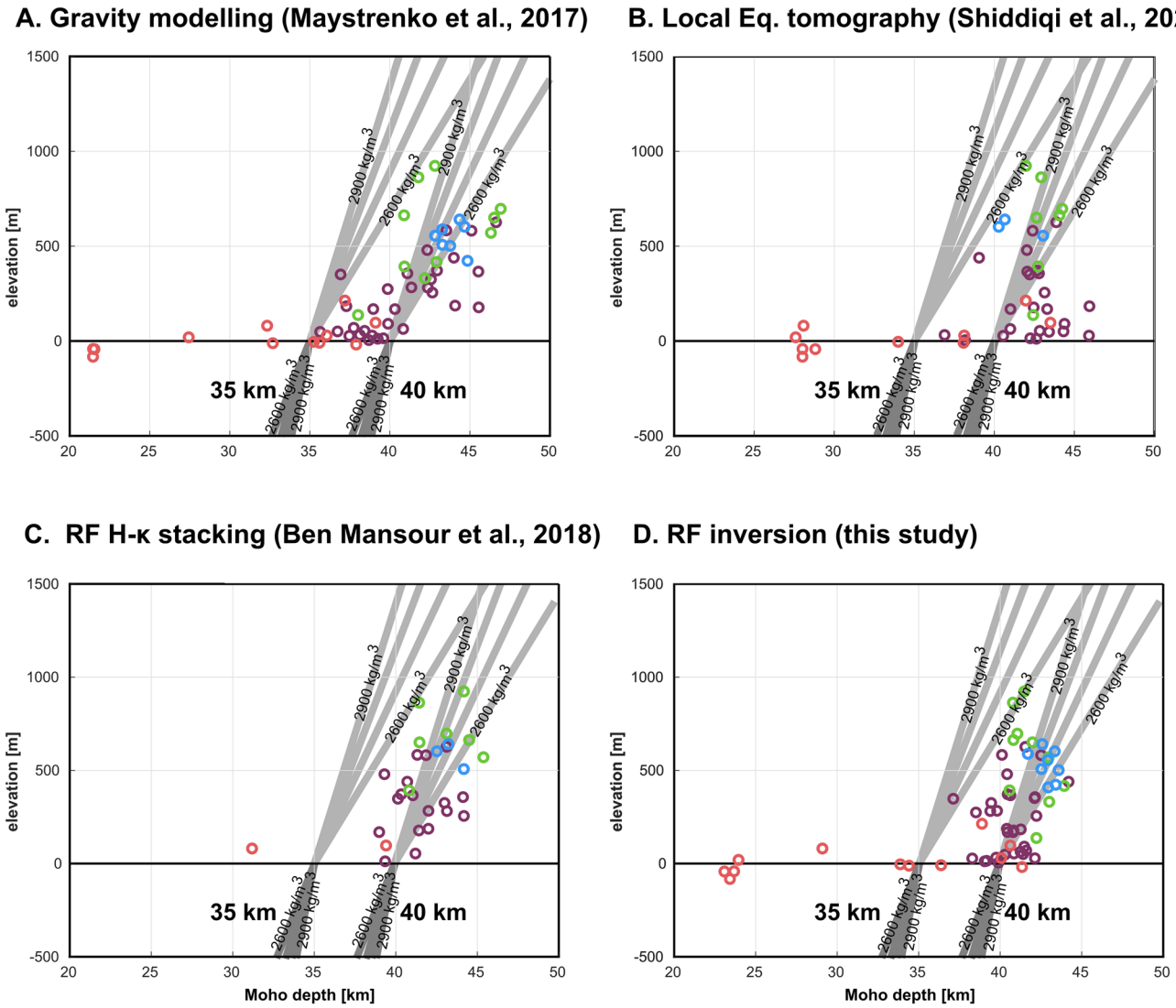

Figure 8. Estimated crustal thickness in comparison with topographic elevation of the four compared models: (a) Maystrenko et al. (2017); (b) Shiddiqi et al. (2022), (c) Ben Mansour et al. (2018) and (a) this study. The values are plotted at every station location used in this study (if the model covers the area). The topography and crustal thickness are averaged in an area with 10 km radius around every station location. The gray lines show theoretical Airy-isostatic compensation relationships for 35 and 40 km compensation depth and crustal densities of 2,600, 2,700, 2,800, and 2,900 kg/m^3 for marine and land areas (dark and light, respectively). The results are shown as color-coded circles according to a very coarse zonation of the area based on bedrock geology: red—Lofoten-Vesterålen archipelago; purple—Caledonian Uppermost Allochthon; green—Caledonian Upper Allochthon; Blue—Caledonian Middle Allochthon and Fennoscandian shield.

Allochthon (purple) forms an anomaly (the low topography is inconsistent with the thick crust observed) and appears to extend the nearly flat trend of the crust in the Lofoten-Vesterålen archipelago. Lastly, the results from RF analyses by Ben Mansour et al. (2018) and Ottemöller et al. (2018) (Figure 8c) suggest an overall isostatic state very similar to our model, with the caveat that only one estimate for the Lofoten-Vesterålen archipelago is available.

In conclusion, all models show that while the topography in the Lofoten-Vesterålen archipelago does not vary considerably, the crustal thickness varies by ∼15 km. Such a change in crustal thickness could be compensated by an equivalent density change of >300 kg/m^3 only within the crust. We observe a low-velocity (and probably low-density) UML, which may provide additional buoyancy. This will be further explored in test 2 below. The Scandinavian mainland generally shows a much better, yet still imperfect, fit to simple Airy-type crustal isostasy with crustal thicknesses scattered about an apparent mean compensation depth of ∼40 km.

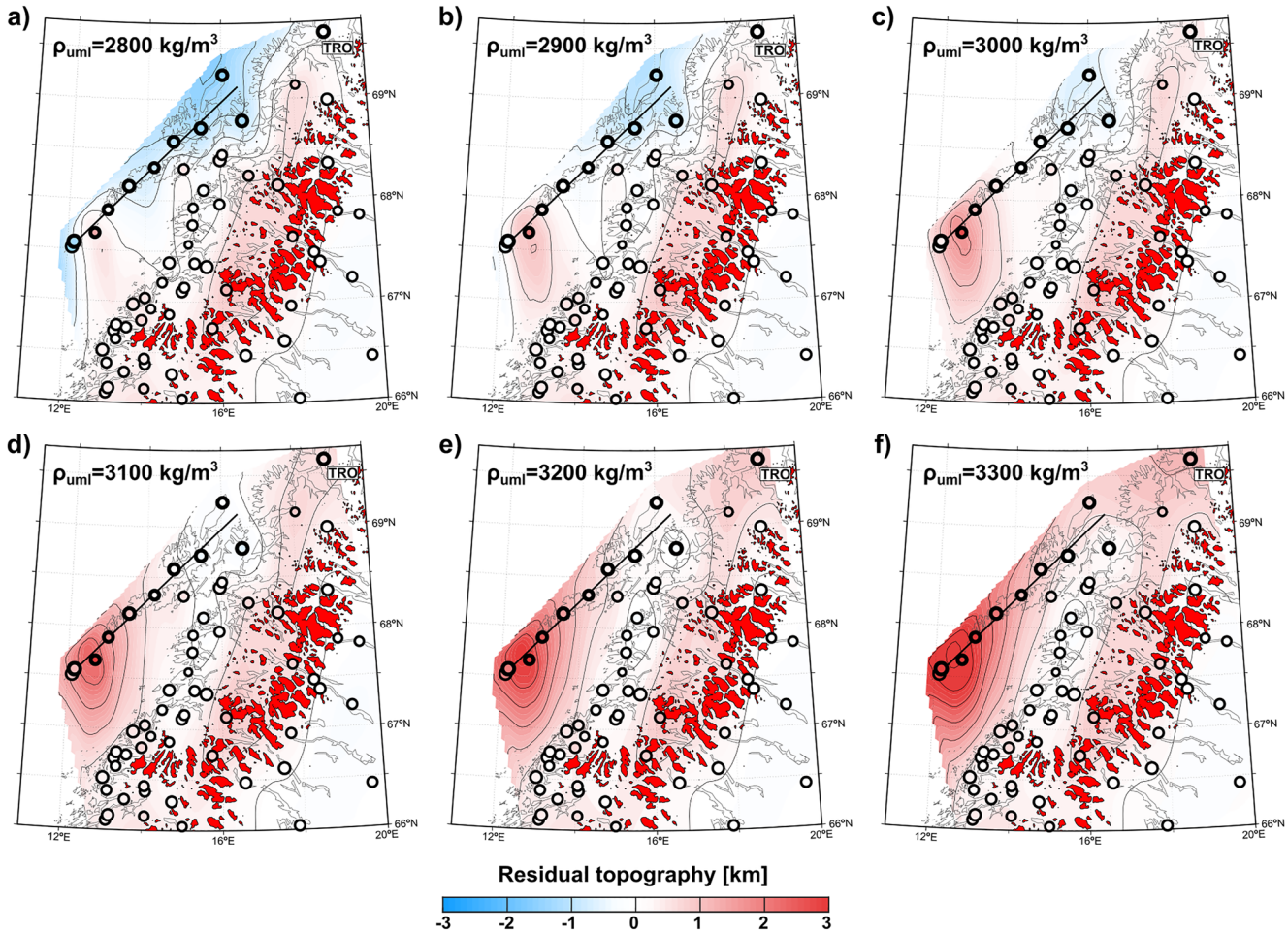

Figure 9. Residual topography maps of the study area considering crustal thickness and the additional upper mantle layer (uml) beneath the northwestern stations (thicker circles). Black isolines are placed at 500 m steps. Red polygons show the area of topography higher than 1,000 m. To calculate the residual topography, the topography is calculated at every station using local crustal isostasy with a density of 2,800 kg/m^3 and a compensation depth of 40 km. For 11 stations the additional uml is included in the isostatic calculation with varying densities (ρ_{uml}) from 2,800 to 3,300 kg/m^3 (a–f). A ρ_{uml} of 2,800 kg/m^3 (a) simply represents crustal densities to the depth of the uml, whilst a ρ_{uml} of 3,300 kg/m^3 (f) represents the reference mantle density meaning only crustal isostasy, without any effect from the uml. For the 11 stations, a clear north-south variation can be observed: the southern stations (ROES, N2RO, N2SV, LOF) with exception of one station, which might be an outlier (N2VA) show overall the best fit for a ρ_{uml} of approx. 2,900 kg/m3; the northern stations (N2VI, N2BR, N2SO, N2HA, N2AN) have the overall best fit for ρ_{uml} of approx. 3,100 kg/m3, both densities, however, are lower than the reference mantle. Isostatic calculations for the stations in the inland also show an up to 1,000 m too high topography, suggesting that buoyancy from other sources may be required to explain the topography.

2. Next, we investigate residual topography of the region by taking into account the low-velocity UML detected by our analysis at 11 stations beneath the Lofoten archipelago (Figure 9). The UML has a lower boundary at ~45–50 km and is estimated to have low Vs compared to typical mantle. It is likely associated with low-density rocks with respect to the mantle (e.g., Christensen & Mooney, 1995), in which case it provides additional buoyancy. The mantle lithosphere in the gravity model by Maystrenko et al. (2017) exhibits slightly lower densities beneath the Lofoten Ridge and islands, which may be related to the structure detected by our study. Here we show that this low density may be confined to the UML above ~50 km depth, rather than being distributed over the whole mantle lithosphere column.

   The residual topography is defined by the difference between observed and locally balanced topography assuming Airy isostasy—a positive value indicating that the topography is too high to be explained by the isostatic model and vice versa. For the isostatic calculations, we again use a density of 3,300 kg/m^3 for the upper mantle and 2,800 kg/m^3 for the crust—values that provided a good fit in test 1 but are surely not the only possible combination. We then vary the density for the UML (ρ_{uml}) between these two end-members (2,800 kg/m^3—equivalent to crust—and 3,300 kg/m^3—equivalent to reference mantle). This clearly is a

simplified model of the crust/mantle lithosphere system, but it can nonetheless provide useful insight into regional isostatic trends and a rough idea about possible density variations in the UML.

The different residual topography models for the tested ρ_{uml} values are shown in Figure 9. Differences in the maps can only be seen for the 11 stations across the Lofoten-Vesterålen archipelago and the station in Tromsø—that is, the only stations at which a substantial UML was observed. The analysis illustrates a stark contrast between the stations located in southern versus northern Lofoten Ridge. The best fit for the stations in the south (N2RO, ROEST, N2SV, LOF, N2VI) is observed when using an UML density of ~2,900–3,000 kg/m^3, which is 100–200 kg/m^3 denser than the reference crust. We consider the only exception (N2VA), as a possible local outlier, as station N2VA also has a relatively shallow lower UML boundary of ~35 km, which could be a misinterpretation. In contrast, the northern stations (N2BR, N2SO, N2HA, N2AN) show the best fit for an UML density of ~3,100 kg/m^3, clearly higher than the best fit for the southern stations, but still 200 kg/m^3 lower than reference mantle. Station TRO shows the best fit using the crustal reference density (2,800 kg/m^3), which might imply that the Moho is deeper here and was misinterpreted. On the mainland, we observe a coast-parallel region that appears to have an average of ~300 m excess topography over values suggested by local crustal isostasy using our crustal model, which would require an additional source of buoyancy as well. This region roughly coincides with the area occupied by the Caledonian Upper Allochthon, where we observe the highest topography and locally shallow Moho, according to our receiver function results. However, across the entire southern end of the study area, the crust of the mainland seems to be in local isostatic balance according to our parameterization, possibly hinting toward a change in crustal properties across ~66.5°N, which roughly corresponds to the onshore extrapolation of the Bivrost lineament across the Norwegian margin offshore.

Test 2 illustrates the possibility for the UML to contribute to the isostatic compensation of the lithosphere in the region. How large this contribution may be in reality remains an open question and depends on the actual density distribution in the crust. For example, as mentioned above in Section 2.2, previous studies have suggested lower densities beneath the Lofoten-Vesterålen archipelago (e.g., Maystrenko et al., 2017).

5. Discussion

Our results provide important new constraints on the architecture of the crust and upper mantle in Nordland and Troms, with new independent evidence for extremely thin crust below southern Lofoten, and the discovery of an UML layer that gives new insight into the lithospheric stratification and isostatic state of the region. We will first discuss some uncertainties and general features of the model and follow with a discussion of the crust/upper mantle structure and isostasy in the study area.

5.1. Uncertainties, Errors, and Trends

In the Supplementary Information, we present a full set of graphs showing data and model uncertainties for every individual model (Figures S1 in Supporting Information S1) and station averages (Figures S2 and S3 and Table S1 in Supporting Information S1). The data uncertainties, that is, the standard deviations observed in the RF stacks and the Vs_{app} curves, range from very small (0.055 and 0.48 km/s, respectively) to considerably large (0.109 and 1.89 km/s) values between the stations. As expected, most permanent stations exhibit standard deviations that are below average, with the exception of stations LEIR and NIKU, which have higher RF uncertainties but low Vs_{app} standard deviations. As already mentioned in Section 3.1, station LOF has extremely low amplitudes at P-wave arrival. The reason for this anomalous result may be that the station is located on top of a Moho step (Figure 2), which affects the incidence angles and wave polarizations, causing a departure from the horizontal layer approximation that cannot be accounted for by our approach in its current form. Indeed, we notice a strong azimuthal variation of the Z-R ratio at station LOF. Interestingly, station LOF exhibits no abnormally large standard deviation for any of the data, despite having abnormally low Vs_{app} values. The fact that the data quality appears to be good, the reason for the unrealistic data is probably structural complexity in the sub-surface. To address this issue, we doubled the a priori data error for Vs_{app} at station LOF. The inversion should take care of this larger data error, which may result in a higher a posteriori model uncertainty. Indeed, LOF shows a much larger standard deviation of the model distribution compared to other permanent stations. However, because LOF yields very similar results to previous models, we are very confident in our result.

We investigate three measures of uncertainty that may represent the quality of the individual models resulting from the inversion: (a) the Moho uncertainty read from the standard deviations of the model population (Figure S3a in Supplementary information S1), (b) the thickness of the interpreted crust-mantle transition zone, which may lead to an interpretation error of the exact Moho depth as a singular value (Figure 3b in Supplementary information S1), and (c) the average velocity uncertainty based on the standard deviations of the velocity model population (Figure 3c in Supplementary information S1). The uncertainty represented by measure (a) varies from 1.6 to 6.6 km, with only three stations showing an uncertainty larger than 5 km. Uncertainties based on measure (b) range from 0.5 to 5 km. Finally, the average velocity uncertainty based on measure (c) ranges from 0.1 to 0.2 km/s. The Moho depth uncertainties partly represent the fact that we observe thick crust-mantle transition zones, which make the definition of one singular Moho depth value difficult or in fact impossible, thus, we can observe a correlation between the uncertainty measures (a) and (b). The velocity uncertainty (measure c) appears to be more scattered across the study area. Smoothing our results to create grids therefore gives a regional representation of the crustal structure, through which we may lose some detail, but also average out these random errors. We are confident that the regional crustal structure within the resolution of this smoothing process is robust. There seems to be only a weak correlation between data errors and estimated model uncertainties (Table S1 in Supporting Information S1), which indicates that the various model uncertainties are not only a product of data quality, but can also stem from geological complexity.

The local differences in Moho depth between the four crustal models shown in Figure 2 in the range of typically up to ∼5 km (Figure 5), both onshore and offshore, could partly reflect these model uncertainties. Additionally, we observe different average crustal thicknesses between the stations, as mentioned in Section 4.1. These local and average differences could also reflect the structural complexity of the crust-mantle transition, the exact definition of the Moho in the different studies, as well as different sensitivities of the employed methods (discontinuity vs. gradient; density, *Vs* or *Vp*).

For example, the Moho based on the tomography model will require some kind of velocity threshold or gradient, similar to our definition. H-κ stacking relies on a fully automatic Moho depth estimation, not accounting for any gradual Moho and furthermore requires a choice of average crustal *Vp*. Refraction models are usually the product of forward modeling schemes. Depending on the modeler and the exact choice of velocities, number of layers and gradients, systematic changes may be introduced. The underlying problem is how the Moho is expressed in geophysical properties and how it is interpreted between various models with different resolution. We observe that the gravity model tends to result in thinner crust along the coastline compared to our study, a similar tendency as that observed in a recent study in the Northwest Atlantic comparing RF crustal models with gravity-derived crustal models (Schiffer et al., 2022).

Nevertheless, we argue that disagreement in Moho depth estimates between estimates based on different geophysical properties (*Vs*, *Vp*, density) could be used as a tool for interpretation. Differences in Moho depth can provide information about *Vp*/*Vs* ratios and velocity-density relationships, and thereby add inferences about rock types, presence of fluids or temperatures in the lower crust/upper mantle. We note that it is important to retain information about the Moho structure, that is, the thickness and gradients within the crust-mantle transition.

5.2. Tectonic Implications

The most striking feature of our model is the transition from a Moho depth of ∼20 km on the Lofoten Ridge to more than ∼35 km in the northern Lofoten-Vesterålen archipelago, as well as a low-velocity layer in the upper mantle directly beneath the crust in the same area (UML). The change in Moho depth appears to be in large parts accommodated by an abrupt step located beneath the southern tip of the Lofoten, between ∼68.00°N and 68.25°N. This step is also observed in other models of the region (Maystrenko et al., 2017; Shiddiqi et al., 2022), but at slightly different locations and with different steepness. The crust along the Lofoten-Vesterålen archipelago and Lofoten Ridge is not in full isostatic equilibrium, which is supported by all models studied here: while the Moho depth increases from ∼20 to ∼40 km, the corresponding averaged topography only shows very minor variations of typically less than 300 m. Unrealistic density changes would be required to compensate these crustal thickness variations. Therefore, the isostatic support in the southern Lofoten, where the crust is thinnest, must come from elsewhere than within the crust (e.g., mantle lithosphere, sub-lithospheric processes or flexural effects), confirming previous studies (Gradmann et al., 2017; Maystrenko et al., 2017). Indeed, it appears that the

seismicity focusses between the putative area of unsupported topography in the Lofoten-Vesterålen archipelago and the area of supported topography in the mainland (e.g., Shiddiqi et al., 2022).

One possible modification of the isostatic state in this area could be the thick lithosphere in the Lofoten-Vesterålen archipelago (Lebedev et al., 2018; Schiffer et al., 2018), potentially resulting in a large elastic thickness (Struijk et al., 2018), strong enough to carry the crust and reducing the effect of crustal thickness variations. Both Hejrani et al. (2020) and Bulut et al. (2022) identified a low velocity anomaly at ∼100–200 km depth beneath the Lofoten margin that may relate to lithospheric structure or sub-lithospheric dynamic processes affecting the isostatic state of the region. In contrast, regional tomography models (Celli et al., 2021; Rickers et al., 2013) do not indicate a substantial low-velocity anomaly in these depth range. Independent dynamic topography estimates in the region appear not to be large and, in fact, slightly negative (Flament et al., 2013; Schiffer & Nielsen, 2016). Both a thick strong lithosphere and dynamic topography would have a regional effect on the topography.

Our results suggest another possible candidate to explain the non-isostatic component, in the form of a low-velocity (and likely low-density) layer observed in the uppermost mantle beneath the Lofoten Ridge and Lofoten-Vesterålen archipelago (the UML). The surprisingly continuous lower boundary of this layer at ∼45 km depth is particularly interesting, as the crustal isostatic compensation depth in the mainland to the east appears to be at a similar depth. Considering the assumptions made (reference densities, compensation depth) and the uncertainties for layer thickness, our isostatic tests appear robust and confirm that low mantle densities of 2,800–3,100 kg/m^3 in this layer may be a viable source of isostatic compensation for the topography in the Lofoten-Vesterålen archipelago. Whether this layer provides all the necessary buoyancy, in southern Lofoten, or only partly, cannot be determined in this study. This structure is spatially coincident with a zone of low densities in the mantle lithosphere inferred from gravity modeling (Maystrenko et al., 2017), as well as with a deeper low velocity anomaly in the upper mantle (Hejrani et al., 2020). To determine the different contributions from various sources to explain the topography would require a comprehensive, integrated geophysical-geodynamic modeling analysis of the region considering isostasy, dynamic effects, elasticity, gravity, lithospheric structure and other data.

At this point, we can only speculate about the origin of this UML, but given its near constant depth of ∼45 km we suggest that it is a regional feature. Its morphology implies that the UML may have been able to adapt to the Moho architecture, "filling in" Moho undulations. Such a behavior hints to a ductile rather than rigid material, or to a velocity/density change dictated by depth/pressure conditions. A possible candidate of such rheology is a layer of hydrated/serpentinized mantle that "underplated" the crust and adjusted to Moho depth undulations above. The lower boundary could represent the hydration front. Similar observations in East Greenland (Schiffer et al., 2015), the North Sea (Fichler et al., 2011) and SW Norway (Slagstad et al., 2018) have been interpreted as hydrated upper mantle/serpentinite structures from former subduction complexes, and could be a prevailing feature in rifted margins or former collision zones. The discontinuity could also represent a phase transition, with possible candidates being eclogitization of lower crustal material or the transition of peridotite from spinel into garnet facies. We think it is unlikely to have crustal material present at 45–50 km. To create a visible seismic discontinuity in a peridotite, a sufficiently "enriched" peridotite composition (i.e., higher Na, but especially Al content) would be necessary (e.g., Simon & Podladchikov, 2008). High enough temperatures and fluids may explain the relatively shallow depth of the transition, but prior to rifting the depth was likely considerably larger (e.g., Froitzheim et al., 2016). Another possible candidate is lower crustal material that, when heated up, may be able to flow and form this layer with a sub-horizontal lower boundary (e.g., Petersen et al., 2018). In this case, a very large amount of crustal material would be required to fill the whole depth interval. The observed velocities, however, are not consistent with that of lower crust. We emphasize that we currently do not have the necessary evidence to robustly interpret the nature of the UML and more work is required.

We observed distinct HVLC bodies in the study area, in particular beneath the Lofoten-Vesterålen archipelago, as well as a N-S oriented structure branching out from the central Lofoten islands to the south at ∼15°E and a general increase in HVLC thickness in the eastern part of the study area. HVLC observed in different tectonic settings, including rifted continental margins, collision zones and cratonic areas, may exhibit uniform or overlapping geophysical properties (*Vs*, *Vp*, density), yet its origin and composition may differ. Although our study is not focused on HVLC origin, it is possible that the HVLC in the Lofoten-Vesterålen archipelago is related to rifting and/or breakup along the LVCM. It may therefore be linked to either rift related magmatism (Thybo & Artemieva, 2013) or deformed pre-existing structures (Petersen & Schiffer, 2016). The HVLC in the mainland part of the study area may be the same HVLC as observed in other Precambrian crust in Fennoscandia, the exact

composition and origin of which is debated (England & Ebbing, 2012; Kolstrup & Maupin, 2013; Kukkonen et al., 2008; Schmidt, 2000). The observation of the N-S oriented structure branching out to the south from the Lofoten-Vesterålen archipelago is puzzling and we do not yet have a good explanation for it. The fact that the presence of HVLC here coincides with a deeper Moho, however, could either mean that HVLC was added (by underplating or intrusions), or that it represents a rheology more resistant to crustal thinning, for instance during post-Caledonian extension.

Along the coastline (Uppermost Allochthon) and in the shield area of the Scandinavian mainland we observe a deeper Moho, a generally thicker HVLC and a smoother crust-mantle transition expressed by small Moho gradients. The crust in this area appears to be largely in isostatic equilibrium (with the given assumptions). In contrast, along a SSW-NNE oriented stretch comprising the highest topography roughly following the area occupied by the Upper Allochthon, the Moho is slightly shallower, HVLC is thinner, the crust-mantle transition sharper, and the topography appears to be undercompensated in a simplified Airy-isostatic model (crust is too thin to explain the topography). This hints to a strong control of Caledonian and Precambrian terranes on the topography. One way of explaining the "too high" topography in the Upper Allochthon in the northern part of the study area versus the "more compensated" crust beneath the Uppermost Allochthon and the Precambrian shield could be density differences within in the crust or lithospheric mantle.

Kolstrup and Maupin (2013) interpreted low Moho gradients in areas of Palaeoproterozoic bedrock as partially eclogitized mafic underplating. Ben Mansour et al. (2018) used Ps/P amplitude ratio as a measure for Moho sharpness, which shows a very similar regional pattern in the overlapping study area: a sharper Moho along the southern coastline, transitioning to a more diffuse Moho in a S-N oriented band between ∼15° and 16°E, followed by two regions of alternating sharp and diffuse Moho in the interior of Fennoscandia. Both Ben Mansour et al.'s (2018) and our model have a strong coast/Caledonian-parallel strike of these Moho sharpness domains, with the sharpest Moho occurring beneath the region of highest topography in the Upper Allochthon, which was not captured to same extent by the other models.

In closing this section, it should be noted that our isostatic calculations are approximate, as they assume simple, local, crustal Airy compensation. Indeed, many other effects contribute to isostasy and/or the support of topography, such as lateral density variations within the crust, lithospheric thickness and density structure, the elastic thickness of the lithosphere, as well as sub-lithospheric dynamic effects, which we don't consider here. Looking at the gravity anomalies in the region (e.g., Ebbing, 2007; Maystrenko et al., 2017), two-large-amplitude anomalies are observed. The first is a dominant positive anomaly along the Lofoten-Vesterålen archipelago, suggesting a mass excess and supporting the model of undercompensated topography (high topography inconsistent with the thin crust). The second is an enigmatic negative anomaly on the mainland, parallel to the Lofoten islands, the origin of which is essentially unknown (Gradmann & Ebbing, 2015). This, and various previous studies (e.g., Gradmann & Ebbing, 2015; Gradmann et al., 2017; Maystrenko et al., 2017), show that the gravity anomalies and the state of isostasy are not trivial in the Nordland and Troms region, and that a solution to the incompatibility between the imaged crustal structure, the topography and the gravity has not yet been found. Our study provides new insights into the lithospheric structure of the area, and especially a more complex stratification of the crust-mantle transition zone, that should be incorporated into future models.

6. Conclusions

Our new crustal model of the Nordland and Troms region provides important new insight into the lithospheric structure, geodynamic evolution and isostasy in the region, while being complementary to previous geophysical studies of the area. The model confirms the existence of a thin crust beneath southern Lofoten and an abrupt crustal thickening toward central Lofoten and Vesterålen. The Moho depths along the Lofoten-Vesterålen islands do not agree with local crustal isostasy. Additional support may come from other effects, such as lithospheric density and thickness variations, the lithospheric strength or sub-lithospheric processes. Our results have confirmed pre-existing crustal thickness models of the region, but have also presented new evidence for an important structural element (the UML) in the uppermost mantle that may provide the additional support for the high topography along the southern Lofoten islands. Our isostatic calculations show that even with a simplified assumption of local Airy isostasy, the region's topography can to a large degree be explained by crustal isostasy, with the exception of the southern Lofoten, where other contributions to isostasy are required. In such regions of apparent

isostatic imbalance of the crust, compensation may come from the structure of the wider crust-mantle transition. As we have shown for Nordland, this transition cannot be viewed here as a simple sharp Moho interface between crustal and mantle rocks, but rather as a gradational zone that potentially comprises layers of high-velocity lower crustal material and/or underplated mantle rocks. This is a view of the Moho that should be adopted not only in rifted margins but also in other tectonic environments where the reactivation of pre-existing structured and the addition of new material can reshape the Moho over time. The paradoxical relationship between Moho depth and architecture, surface topography and gravity field, as well as the origin of the observed upper mantle layer presented here raise a number of issues that should be investigated in future studies. Furthermore, our model suggests a rather strong relationship between the Caledonides and the underlying crustal structure showing a strong orientation parallel to the coast and Caledonian surface structures. An integration of all available geophysical results, the geology, detailed isostatic analysis in combination with petrological modeling may shed further light on the structure and isostatic state of the lithosphere in the northern Norway.

Data Availability Statement

Raw data from several temporary and permanent networks were used, including the Norwegian National Seismic Network (NNSN, Ottemöller et al., 2018, https://doi.org/10.7914/SN/NS), the Swedish National Seismic Network (SNSN, Lund et al., 2021, https://doi.org/10.18159/SNSN) and the temporary networks ScanArray (Thybo et al., 2012, 2021, https://doi.org/10.14470/6T569239), NEONOR2 (Michálek et al., 2018), SCANLIPS2 and SCANLIPS3D (Ben Mansour et al., 2018, https://doi.org/10.7914/SN/ZR_2013; England, 2013; England & Ebbing, 2012). Data were extracted from IRIS (https://ds.iris.edu/ds/nodes/dmc/forms/breqfast-request/) and EIDA Orfeus (http://www.orfeus-eu.org/data/eida/). We obtained teleseismic earthquake catalogue data from the United States Geological Survey (USGS). The data were processed using MATLAB. Figures were made using the Matlab toolbox m_map and inkscape.

Acknowledgments

CS is funded by the Swedish Research Council (Vetenskapsrådet, 2019-04843). Global Lithospheric Imaging with Earthquake Recordings (GLImER) was funded by a Marie Skłodowska Curie—Career Integration Grant 321871 from the European Commission FP7 Programme to SR. SR and LO contributed to this work as part of the Norwegian Research Council funded project on Intraplate Seismicity in India and Norway (IPSIN, project 248815). We thank Sofie Gradmann and an anonymous reviewer for valuable, critical and constructive comments that helped improving this article. We thank Max Moorkamp and Michael Bostock for handling this contribution.

References

Amante, C., & Eakins, B. W. (2009). ETOPO1 1 arc-minute global relief model: Procedures, data sources and analysis. *NOAA Technical Memorandum NOS-NGS*, *24*. https://doi.org/10.7289/V5C8276M

Ammon, C. J. (1991). The isolation of receiver effects from teleseismic P waveforms. *Bulletin of the Seismological Society of America*, *81*(6), 2504–2510. https://doi.org/10.1785/bssa0810062504

Ammon, C. J., Randall, G. E., & Zandt, G. (1990). On the nonuniqueness of receiver function inversions. *Journal of Geophysical Research: Solid Earth*, *95*(B10), 15303–15318. https://doi.org/10.1029/JB095iB10p15303

Avedik, F., Berendsen, D., Fucke, H., Goldflam, S., & Hirschleber, H. (1984). *Seismic investigations along the Scandinavian «Blue Norma» profile* (pp. 571–577). Annales geophysicae.

Ben Mansour, W., England, R. W., Fishwick, S., & Moorkamp, M. (2018). Crustal properties of the northern Scandinavian mountains and Fennoscandian shield from analysis of teleseismic receiver functions. *Geophysical Journal International*, *214*(1), 386–401. https://doi.org/10.1093/gji/ggy140

Bergh, S. G., Eig, K., Kløvjan, O. S., Henningsen, T., Olesen, O., & Hansen, J.-A. (2007). The Lofoten-Vesterålen continental margin: A multiphase mesozoic-palaeogene rifted shelf as shown by offshore-onshore brittle fault-fracture analysis. *Norwegian Journal of Geology*, *87*.

Blystad, P. (1995). Structural elements of the Norwegian continental shelf. Part 2: The Norwegian Sea region. *NPD Bulletins*, *8*.

Bradley, D. C. (2008). Passive margins through Earth history. *Earth-Science Reviews*, *91*(1–4), 1–26. https://doi.org/10.1016/j.earscirev.2008.08.001

Breivik, A. J., Faleide, J. I., Mjelde, R., Flueh, E. R., & Murai, Y. (2017). A new tectono-magmatic model for the Lofoten/Vesterålen Margin at the outer limit of the Iceland Plume influence. *Tectonophysics*, *718*, 25–44. https://doi.org/10.1016/j.tecto.2017.07.002

Breivik, A. J., Faleide, J. I., Mjelde, R., Flueh, E. R., & Murai, Y. (2020). Crustal structure and erosion of the Lofoten/Vesterålen shelf, northern Norwegian margin. *Tectonophysics*, *776*, 228318. https://doi.org/10.1016/j.tecto.2020.228318

Bulut, N., Thybo, H., & Maupin, V. (2022). Highly heterogeneous upper-mantle structure in Fennoscandia from finite-frequency P-body-wave tomography. *Geophysical Journal International*, *230*(2), 1197–1214. https://doi.org/10.1093/gji/ggac107

Celli, N. L., Lebedev, S., Schaeffer, A. J., & Gaina, C. (2021). The tilted Iceland Plume and its effect on the North Atlantic evolution and magmatism. *Earth and Planetary Science Letters*, *569*, 117048. https://doi.org/10.1016/j.epsl.2021.117048

Cherevatova, M., Smirnov, M. Y., Korja, T., Pedersen, L. B., Ebbing, J., Gradmann, S., et al. (2015). Electrical conductivity structure of north-west Fennoscandia from three-dimensional inversion of magnetotelluric data. *Tectonophysics*, *653*, 20–32. https://doi.org/10.1016/j.tecto.2015.01.008

Christensen, N. I. (1996). Poisson's ratio and crustal seismology. *Journal of Geophysical Research: Solid Earth*, *101*(B2), 3139–3156. https://doi.org/10.1029/95JB03446

Christensen, N. I., & Mooney, W. D. (1995). Seismic velocity structure and composition of the continental crust: A global view. *Journal of Geophysical Research: Solid Earth*, *100*(B6), 9761–9788. https://doi.org/10.1029/95JB00259

Clayton, R. W., & Wiggins, R. A. (1976). Source shape estimation and deconvolution of teleseismic bodywaves. *Geophysical Journal of the Royal Astronomical Society*, *47*(1), 151–177. https://doi.org/10.1111/j.1365-246X.1976.tb01267.x

Doré, A. G., & Lundin, E. R. (1996). Cenozoic compressional structures on the NE Atlantic margin; nature, origin and potential significance for hydrocarbon exploration. *Petroleum Geoscience*, *2*(4), 299–311. https://doi.org/10.1144/petgeo.2.4.299

Doré, A. G., Lundin, E. R., Fichler, C., & Olesen, O. (1997). Patterns of basement structure and reactivation along the NE Atlantic margin. *Journal of the Geological Society*, *154*(1), 85–92. https://doi.org/10.1144/gsjgs.154.1.0085

Drivenes, G., Sellevoll, M. A., Renard, V., Avedik, F., & Pajchel, J. (1984). The continental margin/crustal structure off the Lofoten Islands, Northern Norway. In *Petroleum geology of the North European margin* (pp. 211–216). Springer.

Ebbing, J. (2007). Isostatic density modelling explains the missing root of the Scandes. *Nor. J. Geol.*, *87*, 13–20.

Ebbing, J., & Olesen, O. (2005). The Northern and southern scandes — Structural differences revealed by an analysis of gravity anomalies, the geoid and regional isostasy. *Tectonophysics*, *411*(1–4), 73–87. https://doi.org/10.1016/j.tecto.2005.09.002

England, R. (2013). SCANLIPS3D [Dataset]. International Federation of Digital Seismograph Networks. https://doi.org/10.7914/SN/ZR_2013

England, R. W., & Ebbing, J. (2012). Crustal structure of central Norway and Sweden from integrated modelling of teleseismic receiver functions and the gravity anomaly. *Geophysical Journal International*, *191*, 1–11. https://doi.org/10.1111/j.1365-246X.2012.05607.x

Færseth, R. B. (2012). Structural development of the continental shelf offshore Lofoten–Vesterålen, northern Norway. *Norwegian Journal of Geology*, *92*.

Fichler, C., Odinsen, T., Rueslåtten, H., Olesen, O., Vindstad, J. E., & Wienecke, S. (2011). Crustal inhomogeneities in the Northern North Sea from potential field modeling: Inherited structure and serpentinites? *Tectonophysics*, *510*(1–2), 172–185. https://doi.org/10.1016/j.tecto.2011.06.026

Flament, N., Gurnis, M., & Müller, R. D. (2013). A review of observations and models of dynamic topography. *Lithosphere*, *5*(2), 189–210. https://doi.org/10.1130/L245.1

Fossen, H. (2010). Extensional tectonics in the North Atlantic Caledonides: A regional view. *Geol. Soc. Lond. Spec. Publ.*, *335*(1), 767–793. https://doi.org/10.1144/sp335.31

Franke, D. (2013). Rifting, lithosphere breakup and volcanism: Comparison of magma-poor and volcanic rifted margins. *Marine and Petroleum Geology*, *43*, 63–87. https://doi.org/10.1016/j.marpetgeo.2012.11.003

Froitzheim, N., Miladinova, I., Janák, M., Kullerud, K., Ravna, E. K., Majka, J., et al. (2016). Devonian subduction and syncollisional exhumation of continental crust in Lofoten, Norway. *Geology*, *44*(3), 223–226. https://doi.org/10.1130/g37545.1

Gee, D. G. (2015). Caledonides of Scandinavia, Greenland, and Svalbard. In *Reference module in Earth systems and environmental sciences*. Elsevier.

Gernigon, L., Franke, D., Geoffroy, L., Schiffer, C., Foulger, G. R., & Stoker, M. (2020). Crustal fragmentation, magmatism, and the diachronous opening of the Norwegian-Greenland Sea. *Earth-Science Reviews*, *206*, 102839. https://doi.org/10.1016/j.earscirev.2019.04.011

Gernigon, L., Ringenbach, J.-C., Planke, S., & Le Gall, B. (2004). Deep structures and breakup along volcanic rifted margins: Insights from integrated studies along the outer Vøring basin (Norway). *Marine and Petroleum Geology*, *21*(3), 363–372. https://doi.org/10.1016/j.marpetgeo.2004.01.005

Goldschmidt-Rokita, A., Sellevoll, M. A., Hirschleber, H. B., & Avedik, F. (1988). Results of two seismic refraction profiles off Lofoten, Northern Norway. *NGU Special Publication Norges Geologiske Undersokelse*, *3*, 49–57.

Gradmann, S., & Ebbing, J. (2015). Large-scale gravity anomaly in northern Norway: Tectonic implications of shallow or deep source depth and a possible conjugate in northeast Greenland. *Geophysical Supplements to the Monthly Notices of the Royal Astronomical Society*, *203*(3), 2070–2088. https://doi.org/10.1093/gji/ggv426

Gradmann, S., Haase, C., & Ebbing, J. (2017). Isostasy as a tool to validate interpretations of regional geophysical datasets–application to the mid-Norwegian continental margin. *Geological Society, London, Special Publications*, *447*(1), 279–297. https://doi.org/10.1144/sp447.13

Hansen, J.-A., Bergh, S. G., & Henningsen, T. (2011). Mesozoic rifting and basin evolution on the Lofoten and Vesterålen Margin, North-Norway; time constraints and regional implications. *Norwegian Journal of Geology*, *91*.

Hejrani, B., Balling, N., Jacobsen, B. H., & Nielsen, S. B. (2020). Is high topography around the North Atlantic supported from the upper mantle? *Journal of Geophysical Research: Solid Earth*, *125*(9), e2020JB019808. https://doi.org/10.1029/2020JB019808

Jacobsen, B. H., & Svenningsen, L. (2008). Enhanced uniqueness and linearity of receiver function inversion. *Bulletin of the Seismological Society of America*, *98*(4), 1756–1767. https://doi.org/10.1785/0120070180

Kierulf, H. P., Steffen, H., Barletta, V. R., Lidberg, M., Johansson, J., Kristiansen, O., & Tarasov, L. (2021). A GNSS velocity field for geophysical applications in Fennoscandia. *Journal of Geodynamics*, *146*, 101845. https://doi.org/10.1016/j.jog.2021.101845

Koistinen, T., Wennerstrøm, M., Nordgulen, Ø., Bogatchev, V., Stephens, M. B., & Korhonen, J. (2001). Geological map of the Fennoscandian shield (Vol. *1*, p. 2).

Kolstrup, M. L., & Maupin, V. (2013). A Proterozoic boundary in southern Norway revealed by joint-inversion of P-receiver functions and surface waves. *Precambrian Research*, *238*, 186–198. https://doi.org/10.1016/j.precamres.2013.10.004

Kukkonen, I. T., Kuusisto, M., Lehtonen, M., & Peltonen, P. (2008). Delamination of eclogitized lower crust: Control on the crust–mantle boundary in the central Fennoscandian shield. *Tectonophysics*, *457*(3–4), 111–127. https://doi.org/10.1016/j.tecto.2008.04.029

Langston, C. A. (1979). Structure under Mount Rainier, Washington, inferred from teleseismic body waves. *Journal of Geophysical Research: Solid Earth*, *84*(B9), 4749–4762. https://doi.org/10.1029/JB084iB09p04749

Lebedev, S., Schaeffer, A. J., Fullea, J., & Pease, V. (2018). Seismic tomography of the Arctic region: Inferences for the thermal structure and evolution of the lithosphere. *Geological Society, London, Special Publications*, *460*(1), 419–440. https://doi.org/10.1144/sp460.10

Ligorría, J. P., & Ammon, C. J. (1999). Iterative deconvolution and receiver-function estimation. *Bulletin of the Seismological Society of America*, *89*(5), 1395–1400. https://doi.org/10.1785/bssa0890051395

Lund, B., Schmidt, P., Shomali, Z. H., & Roth, M. (2021). The modern Swedish National Seismic Network: Two decades of intraplate microseismic observation. *Seismological Research Letters*, 92(3), 1747–1758. https://doi.org/10.1785/0220200435

Luosto, U. (1997). Structure of the Earth's crust in Fennoscandia as revealed from refraction and wide-angle reflection studies. *Geophysica*, *33*, 3–16.

Maystrenko, Y. P., Gernigon, L., & Olesen, O. (2020). Comment on "Crustal structure and erosion of the Lofoten/Vesterålen shelf, northern Norwegian margin. Tectonophysics 776, 228318" by AJ Breivik, JI Faleide, R. Mjelde, ER Flueh, Y. Murai. *Tectonophysics*, *793*, 228605. https://doi.org/10.1016/j.tecto.2020.228605

Maystrenko, Y. P., Olesen, O., Gernigon, L., & Gradmann, S. (2017). Deep structure of the Lofoten-Vesterålen segment of the Mid-Norwegian continental margin and adjacent areas derived from 3-D density modeling. *Journal of Geophysical Research: Solid Earth*, *122*(2), 1402–1433. https://doi.org/10.1002/2016jb013443

Medvedev, S., & Hartz, E. H. (2015). Evolution of topography of post-Devonian Scandinavia: Effects and rates of erosion. *Geomorphology*, *231*, 229–245. https://doi.org/10.1016/j.geomorph.2014.12.010

Menke, W. (1989). *Geophysical data analysis: Discrete inverse theory*. Academic Press.

Michálek, J., Tjaland, N., Drottning, A., Strømme, M. L., Storheim, B. M., Rondenay, S., & Ottemöller, L. (2018). *Report on seismic observations within the NEONOR2 project in the Nordland region: Norway*. Technical report. University of Bergen.

Mjelde, R., Goncharov, A., & Müller, R. D. (2013). The Moho: Boundary above upper mantle peridotites or lower crustal eclogites? A global review and new interpretations for passive margins. *Tectonophysics*, *609*, 636–650. https://doi.org/10.1016/j.tecto.2012.03.001

Mjelde, R., Sellevoll, M. A., Shimamura, H., Iwasaki, T., & Kanazawa, T. (1993). Crustal structure beneath Lofoten, N. Norway, from vertical incidence and wide-angle seismic data. *Geophysical Journal International*, *114*(1), 116–126. https://doi.org/10.1111/j.1365-246X.1993.tb01471.x

Mjelde, R., Shimamura, H., Kanazawa, T., Kodaira, S., Raum, T., & Shiobara, H. (2003). Crustal lineaments, distribution of lower crustal intrusives and structural evolution of the Vøring Margin, NE Atlantic; new insight from wide-angle seismic models. *Tectonophysics*, *369*(3–4), 199–218. https://doi.org/10.1016/s0040-1951(03)00199-9

Mosar, J., Eide, E. A., Osmundsen, P. T., Sommaruga, A., & Torsvik, T. H. (2002). Greenland–Norway separation: A geodynamic model for the North Atlantic. *Norwegian Journal of Geology*, *82*, 282.

Nielsen, S. B., Gallagher, K., Leighton, C., Balling, N., Svenningsen, L., Jacobsen, B. H., et al. (2009). The evolution of Western Scandinavian topography: A review of Neogene uplift versus the ICE (isostasy–climate–erosion) hypothesis. *Journal of Geodynamics*, *47*(2–3), 72–95. https://doi.org/10.1016/j.jog.2008.09.001

Quaternary Geology of Norway, Geological Survey of Norway Special PublicationOlesen, O., Bungum, H., Dehls, J., Lindholm, C., Pascal, C., & Roberts, D. (2013). Neotectonics, seismicity and contemporary stress field in Norway–mechanisms and implications. *Quaternary Geology of Norway, Geological Survey of Norway Special Publication*, *13*, 145–174.

Olesen, O., Lundin, E., Nordgulen, Ø., Osmundsen, P. T., Skilbrei, J. R., Smethurst, M. A., et al. (2002). Bridging the gap between the onshore and offshore geology in Nordland, northern Norway. *Norwegian Journal of Geology*, 82.

Olsson, S., Roberts, R. G., & Bödvarsson, R. (2008). Moho depth variation in the Baltic Shield from analysis of converted waves. *GFF*, *130*(3), 113–122. https://doi.org/10.1080/11035890809453227

Osmundsen, P. T., & Ebbing, J. (2008). Styles of extension offshore mid-Norway and implications for mechanisms of crustal thinning at passive margins. *Tectonics*, *27*(6), TC6016. https://doi.org/10.1029/2007TC002242

Osmundsen, P. T., Redfield, T. F., Anda, E., Hendriks, B. W. H., Henderson, I., Dehls, J., et al. (2010). The tectonic significance of Alpine landscapes in Norway. *J. Geol. Soc. Lond.*, *167*(1), 83–98. https://doi.org/10.1144/0016-76492009-019

Ottemöller, L., & Midzi, V. (2003). The crustal structure of Norway from inversion of teleseismic receiver functions. *Journal of Seismology*, *7*(1), 35–48. https://doi.org/10.1023/A:1021294504092

Ottemöller, L., Strømme, M. L., & Storheim, B. M. (2018). Seismic monitoring and data processing at the Norwegian National seismic Network. *Summ. Bull. Int. Seismol. Cent.*, *52*(I), 27–40. https://doi.org/10.31905/1M97CSYL

Péron-Pinvidic, G., & Manatschal, G. (2010). From microcontinents to extensional allochthons: Witnesses of how continents rift and break apart? *Petroleum Geoscience*, *16*(3), 189–197. https://doi.org/10.1144/1354-079309-903

Petersen, K. D., & Schiffer, C. (2016). Wilson cycle passive margins: Control of orogenic inheritance on continental breakup. *Gondwana Research*, *39*, 131–144. https://doi.org/10.1016/j.gr.2016.06.012

Petersen, K. D., Schiffer, C., & Nagel, T. (2018). LIP formation and protracted lower mantle upwelling induced by rifting and delamination. *Scientific Reports*, *8*(1), 16578. https://doi.org/10.1038/s41598-018-34194-0

Reynisson, R. F., Ebbing, J., Lundin, E., & Osmundsen, P. T. (2010). Properties and distribution of lower crustal bodies on the mid-Norwegian margin. *Geological Society London Petroleum Geology Conference series*, (Vol. 7(1), pp. 843–854). https://doi.org/10.1144/0070843

Rickers, F., Fichtner, A., & Trampert, J. (2013). The Iceland–Jan Mayen plume system and its impact on mantle dynamics in the North Atlantic region: Evidence from full-waveform inversion. *Earth and Planetary Science Letters*, *367*, 39–51. https://doi.org/10.1016/j.epsl.2013.02.022

Roberts, D. (2003). The Scandinavian Caledonides: Event chronology, palaeogeographic settings and likely modern analogues. *Tectonophysics*, *365*(1–4), 283–299. https://doi.org/10.1016/S0040-1951(03)00026-X

Rondenay, S. (2009). Upper mantle imaging with array recordings of converted and scattered teleseismic waves. *Surveys in geophysics*, *30*, 377–405.

Rondenay, S., Spieker, K., Sawade, L., Halpaap, F., & Farestveit, M. (2017). Glimer: A new global database of teleseismic receiver functions for imaging Earth structure. *Seismological Research Letters*, *88*(1), 39–48. https://doi.org/10.1785/0220160111

Schermer, E. R., Redfield, T. F., Indrevær, K., & Bergh, S. G. (2017). Geomorphology and topography of relict surfaces: The influence of inherited crustal structure in the northern Scandinavian Mountains. *Journal of the Geological Society*, *174*(1), 93–109. https://doi.org/10.1144/jgs2016-034

Schiffer, C., Doré, A. G., Foulger, G. R., Franke, D., Geoffroy, L., Gernigon, L., et al. (2020). Structural inheritance in the North Atlantic. *Earth-Science Reviews*, *206*, 102975. https://doi.org/10.1016/j.earscirev.2019.102975

Schiffer, C., Eken, T., Rondenay, S., & Taymaz, T. (2019). Localized crustal deformation along the central North Anatolian Fault Zone revealed by joint inversion of P-receiver functions and P-wave polarizations. *Geophysical Journal International*, *217*(1), 682–702. https://doi.org/10.1093/gji/ggz040

Schiffer, C., Jacobsen, B. H., Balling, N., Ebbing, J., & Nielsen, S. B. (2015). The East Greenland Caledonides—Teleseismic signature, gravity and isostasy. *Geophysical Journal International*, *203*(2), 1400–1418. https://doi.org/10.1093/gji/ggv373

Schiffer, C., & Nielsen, S. B. (2016). Implications for anomalous mantle pressure and dynamic topography from lithospheric stress patterns in the North Atlantic Realm. *Journal of Geodynamics*, *98*, 53–69. https://doi.org/10.1016/j.jog.2016.03.014

Schiffer, C., Peace, A. L., Jess, S., & Rondenay, S. (2022). The crustal structure in the Northwest Atlantic region from receiver function inversion – Implications for basin dynamics and magmatism. *Tectonophysics*, *825*, 229235. https://doi.org/10.1016/j.tecto.2022.229235

Schiffer, C., Stephenson, R., Oakey, G. N., & Jacobsen, B. H. (2016). The crustal structure of Ellesmere Island, Arctic Canada—Teleseismic mapping across a remote intraplate orogenic belt. *Geophysical Journal International*, *204*(3), 1579–1600. https://doi.org/10.1093/gji/ggv539

Schiffer, C., Tegner, C., Schaeffer, A. J., Pease, V., & Nielsen, S. B. (2018). High Arctic geopotential stress field and implications for geodynamic evolution. *Geological Society, London, Special Publications*, *460*(1), 441–465. https://doi.org/10.1144/sp460.6

Schmidt, J. (2000). Deep seismic studies in the western part of the Baltic shield. Doctoral dissertation, Acta Universitatis Upsaliensis.

Schulte-Pelkum, V., Mahan, K. H., Shen, W., & Stachnik, J. C. (2017). The distribution and composition of high-velocity lower crust across the continental U.S.: Comparison of seismic and xenolith data and implications for lithospheric dynamics and history. *Tectonics*, *36*(8), 1455–1496. https://doi.org/10.1002/2017TC004480

Sellevoll, M. (1983). A study of the earth's crust in the island area of Lofoten-Vesterålen, Northern Norway.

Shiddiqi, H. A., Ottemöller, L., Rondenay, S., Halpaap, F., Gradmann, S., & Michálek, J. (2022). Crustal structure and intraplate seismicity in Nordland, Northern Norway: Insight from seismic tomography. *Geophysical Journal International*, *230*(2), 813–830. https://doi.org/10.1093/gji/ggac086

Sibuet, J.-C. (1992). New constraints on the formation of the non-volcanic continental Galicia–Flemish Cap conjugate margins. *Journal of the Geological Society*, *149*(5), 829–840. https://doi.org/10.1144/gsjgs.149.5.0829

Silvennoinen, H., Kozlovskaya, E., Kissling, E., & Kosarev, G. (2014). A new Moho boundary map for the northern Fennoscandian Shield based on combined controlled-source seismic and receiver function data. *GeoResJ*, *1–2*, 19–32. https://doi.org/10.1016/j.grj.2014.03.001

Simon, N. S. C., & Podladchikov, Y. Y. (2008). The effect of mantle composition on density in the extending lithosphere. *Earth and Planetary Science Letters*, *272*(1–2), 148–157. https://doi.org/10.1016/j.epsl.2008.04.027

Slagstad, T., Maystrenko, Y. P., Maupin, V., & Gradmann, S. (2018). An extinct, late Mesoproterozoic, Sveconorwegian mantle wedge beneath SW Fennoscandia, reflected in seismic tomography and assessed by thermal modelling. *Terra Nova*, *30*(1), 72–77. https://doi.org/10.1111/ter.12310

Steltenpohl, M. G., Kassos, G., Andresen, A., Rehnström, E. F., & Hames, W. E. (2011). Eclogitization and exhumation of Caledonian continental basement in Lofoten, North Norway. *Geosphere*, *7*(1), 202–218. https://doi.org/10.1130/ges00573.1

Stephenson, R., Schiffer, C., Peace, A., Nielsen, S. B., & Jess, S. (2020). Late Cretaceous-Cenozoic basin inversion and palaeostress fields in the North Atlantic-Western Alpine-Tethys realm: Implications for intraplate tectonics. *Earth-Science Reviews*, *210*, 103252. https://doi.org/10.1016/j.earscirev.2020.103252

Struijk, E. L. M., Tesauro, M., Lebedeva-Ivanova, N. N., Gaina, C., Beekman, F., & Cloetingh, S. A. P. L. (2018). The Arctic lithosphere: Thermo-mechanical structure and effective elastic thickness. *Global and Planetary Change*, *171*, 2–17. https://doi.org/10.1016/j.gloplacha.2018.07.014

Svenningsen, L., & Jacobsen, B. H. (2007). Absolute S-velocity estimation from receiver functions. *Geophysical Journal International*, *170*(3), 1089–1094. https://doi.org/10.1111/j.1365-246X.2006.03505.x

Talbot, C. J. (2001). Weak zones in Precambrian Sweden. *Geological Society, London, Special Publications*, *186*(1), 287–304. https://doi.org/10.1144/gsl.sp.2001.186.01.17

Tarantola, A., & Valette, B. (1982). Generalized nonlinear inverse problems solved using the least squares criterion. *Review of Geophysics*, *20*(2), 219–232. https://doi.org/10.1029/RG020i002p00219

Theilen, F., & Meissner, R. (1979). A comparison of crustal and upper mantle features in fennoscandia and the rhenish shield, two areas of recent uplift. *Tectonophysics*, *61*(1–3), 227–242. https://doi.org/10.1016/0040-1951(79)90299-3

Thybo, H., Balling, N., Maupin, V., Ritter, J., & Tilmann, F. (2012). ScanArray core (1G 2012-2017). https://doi.org/10.14470/6T569239

Thybo, H., & Artemieva, I. M. (2013). Moho and magmatic underplating in continental lithosphere. *Tectonophysics*, *609*, 605–619. https://doi.org/10.1016/j.tecto.2013.05.032

Thybo, H., Bulut, N., Grund, M., Mauerberger, A., Makushkina, A., Artemieva, I. M., et al. (2021). ScanArray—A broadband seismological experiment in the Baltic shield. *Seismol. Soc. Am.*, *92*(5), 2811–2823. https://doi.org/10.1785/0220210015

Tsikalas, F., Eldholm, O., & Faleide, J. I. (2005). Crustal structure of the Lofoten-Vesterålen continental margin, off Norway. *Tectonophysics*, *404*(3–4), 151–174. https://doi.org/10.1016/j.tecto.2005.04.002

Vinnik, L. P. (1977). Detection of waves converted from P to SV in the mantle. *Physics of the Earth and Planetary Interiors*, *15*(1), 39–45. https://doi.org/10.1016/0031-9201(77)90008-5

Zhu, L., & Kanamori, H. (2000). Moho depth variation in southern California from teleseismic receiver functions. *Journal of Geophysical Research: Solid Earth*, *105*(B2), 2969–2980. https://doi.org/10.1029/1999JB900322